mathematics

Article

Data-Driven GWO-BRNN-Based SOH Estimation of Lithium-Ion Batteries in EVs for Their Prognostics and Health Management

Muhammad Waseem [1], Jingyuan Huang [1,*], Chak-Nam Wong [1] and C. K. M. Lee [1,2,*]

1 Centre for Advances in Reliability and Safety (CAiRS), Hong Kong SAR, China; gary.wong@cairs.hk (C.-N.W.)
2 Department of Industrial and Systems Engineering, The Hong Kong Polytechnic University, Hong Kong SAR, China
* Correspondence: jenny.huang@cairs.hk (J.H.); ckm.lee@polyu.edu.hk (C.K.M.L.)

Abstract: Due to the complexity of the aging process, maintaining the state of health (SOH) of lithium-ion batteries is a significant challenge that must be overcome. This study presents a new SOH estimation approach based on hybrid Grey Wolf Optimization (GWO) with Bayesian Regularized Neural Networks (BRNN). The approach utilizes health features (HFs) extracted from the battery charging-discharging process. Selected external voltage and current characteristics from the charging-discharging process serve as HFs to explain the aging mechanism of the batteries. The Pearson correlation coefficient, the Kendall rank correlation coefficient, and the Spearman rank correlation coefficient are then employed to select HFs that have a high degree of association with battery capacity. In this paper, GWO is introduced as a method for optimizing and selecting appropriate hyper-p parameters for BRNN. GWO-BRNN updates the population through mutation, crossover, and screening operations to obtain the globally optimal solution and improve the ability to conduct global searches. The validity of the proposed technique was assessed by examining the NASA battery dataset. Based on the simulation results, the presented approach demonstrates a higher level of accuracy. The proposed GWO-BRNN-based SOH estimation achieves estimate assessment indicators of less than 1%, significantly lower than the estimated results obtained by existing approaches. The proposed framework helps develop electric vehicle battery prognostics and health management for the widespread use of eco-friendly and reliable electric transportation.

Keywords: state of health estimation; lithium-ion batteries; electric vehicles; optimization; prognostics and health management; Grey Wolf Optimizer; battery degradation; data-driven modeling

MSC: 60E05; 62N05

Citation: Waseem, M.; Huang, J.; Wong, C.-N.; Lee, C.K.M. Data-Driven GWO-BRNN-Based SOH Estimation of Lithium-Ion Batteries in EVs for Their Prognostics and Health Management. *Mathematics* **2023**, *11*, 4263. https://doi.org/10.3390/math11204263

Academic Editor: Gaige Wang

Received: 31 August 2023
Revised: 1 October 2023
Accepted: 6 October 2023
Published: 12 October 2023

1. Introduction

Integrating renewable energy sources, electric vehicles (EVs), and smart grid technology is a viable paradigm in the fast-changing environment of contemporary power networks. In tandem with these developments, lithium batteries have assumed a central position in the fields of EVs, smart grids, and microgrids. Lithium batteries' energy storage capacities are significant because they allow for more effective use of renewable power, load balancing, and improved grid stability. They are crucial to the efficient control of energy flows and the stable power supply, allowing for the smooth incorporation of intermittent renewable sources into the grid. In addition, keeping an eye on and servicing lithium batteries in such applications is crucial for keeping them running smoothly and efficiently for as long as possible. New methods for monitoring and controlling lithium batteries have been presented in recent literature [1–5]. These works add to the growing body of knowledge in the field by highlighting the opportunities afforded by sophisticated state-of-health estimation methods and the potential of lithium batteries to revolutionize not only electrified transportation but also the broader scope of smart grid applications. Lithium-ion batteries are often used in EVs owing to their many benefits, including high specific energy, safety, cycle life, low pollution, and self-discharge. Electric vehicles require a battery management system (BMS) for diagnostics, control, and protection [6–9]. The most significant tasks of a BMS are the prediction of the battery's remaining usable life (RUL) and the determination of the battery's state of health (SOH). These capabilities enable users to replace batteries at the appropriate time and minimize disasters caused by batteries. Predicting RUL and SOH is crucial. Battery SOH indicates a battery's age from birth to end of life (EOL). Real capacity/nominal capacity is SOH. The ratio of actual maximum capacity to rated capacity is SOH. When a battery's capacity drops below 70% or 80% of its rated capacity, it is EOL and should be replaced. This capacity figure represents the battery's ultimate failure point. The SOH of a battery provides information on its age and reliability. Because the process of a battery's internal degeneration is so complex, the SOH cannot be assessed directly, and predicting it continues to be challenging despite this [10].

Three classes of battery SOH estimation methods exist. Experimental open-circuit voltage measurements, temperature, and current characterize the battery. Battery SOH and predicted capacity are then calculated [11]. The experimental method only studies one battery type. It is often combined with other methods due to the working environment and equipment precision. The second method estimates battery SOH using state-of-the-art algorithms like Kalman Filter (KF), Particle Filter (PF), and the battery model [12]. Estimating the state of charge (SOC), internal resistance, and SOH of a lithium-ion battery using a hybrid adaptive observer and Enhanced Kalman Filter (EKF) technique is what the authors suggest [13]. In [14], a high-fidelity reduced-order physical life model and PF algorithm simultaneously estimated SOH and aging parameters. The method works well at many temperatures. The model's and filters' precision limits the accuracy and usefulness of battery model-based methods. For the goal of SOH estimation, the data-driven techniques have found significant use since they employ a large number of battery data and do not need any mechanism models or prior knowledge [15]. This is because the data-driven approaches do not need any prior knowledge or information. In recent years, several methods for estimating SOH have emerged, some of which are as follows: neural networks; support vector regression; relevance vector machine; Gaussian process regression; Bayes model; random forest; autoencoder and many more. Most data-driven approaches make use of neural networks as an integral part of their analysis. It's possible that employing this method will be beneficial to batteries and other nonlinear systems. Through the use of the significant sample approach as well as the feedforward neural network, an accurate assessment of the state of the battery was accomplished [16].

A strategy to estimate SOH that makes use of neural networks and Markov chains may be used to handle difficulties that are connected to unknown extreme circumstances as well as sophisticated internal electrochemical reaction processes. The use of data-driven algorithms has expanded as a result of machine learning and big data [17]. Wang et al. [18] used differential thermal voltammetry to determine battery SOH by first extracting parameters from the DTV curve. To estimate the battery's SOH, a gate recurrent unit convolutional NN method that uses charging process voltage, current, and temperature to estimate battery SOH has been proposed by authors in [19]. Authors in [20] proposed an ARMA-ENN fusion model to estimate SOH, taking into account the recovery of local small capacity and the changing of complicated information during charging. The data algorithm works without a battery model. Enough experimental data can also produce highly accurate results for nonlinear systems like batteries [21]. The battery aging behavior was simulated using regression by making use of different fitting functions in [22]. Support vector regression (SVR) and independent component analysis (ICA) curves using incomplete charge data were used in [23]. Similarly, an SVR concept and voltage sub-segments during constant current charging were applied [24]. A Gaussian process regression (GPR) model with charging curve inputs and grey relational analysis has been utilized to assess features and SOH [25]. GPR is used to study lithium-ion battery capacity, storage temperature, and

SOC [26,27]. They forecasted battery calendar aging under diverse settings by optimizing feature selection using an automated relevance determination framework. GPR and electrochemical impedance spectroscopy were used in [28] to estimate battery capacity using numerous waveforms.

Using a Deep Neural Network (DNN), the authors of [29] were able to make predictions about the SOH and RUL of lithium-ion batteries. The SOH and RUL may be predicted using a modified version of the Long and Short-Term Memory (LSTM) NN technique [30]. This approach increased the LSTM NN's ability to digest input and filter out helpful information to improve estimate results. BPNN and an adaptive neural fuzzy reasoning system were applied in [31] to forecast the future performance of proton exchange membrane fuel cells. One of the NN models mentioned above with the most hidden layers is DNN. There are not many studies on DNN, and there are not any references to them either [32]. LSTM-NN has a constant error carousel to prevent error signals from rapidly declining, which would prevent LSTM from learning critical information and impacting network performance [33]. The incapacity of FNN to store and make use of previous data makes the conclusions that were predicted less accurate. In [34], an LMA-ANN and big data analysis were used to try to anticipate the demand for home air conditioning. The approach that was presented is not only more precise but also applicable to a wide variety of time spans. The research demonstrates how the approach works with real-time data and produces performance indices as a result. The Bayesian Regularized Neural Network, often known as BRNN, has a straightforward architecture, is straightforward to compute, and has been improved upon by a large number of academics. The capacity of BRNN to perform error backpropagation in the opposite direction enables the refinement of estimates via parameter fine-tuning [35]. The authors of [36] were able to properly anticipate electricity usage by using instance-based learning of forecast parameters in conjunction with BRNN. The report recommends doing an estimate of the demand for electricity and making sure that the power system is operating efficiently. BRNN has difficulties getting the parameters initialized properly. In order to prevent erroneous predictions caused by weight parameter initialization, it is essential that network parameters be properly selected. Accuracy is essential for forecasting. For more accurate predictions, conventional ANN will need to undergo several improvements. The Grey Wolf Optimization (GWO) algorithm is used in this study to optimize the BRNN weights and thresholds.

Battery performance may be influenced by several aspects in practical scenarios. Numerous studies use the battery charging-discharging procedure as a means to extract Health Features (HFs) that serve as indicators of battery aging, with the aim of predicting SOH. This enables them to make predictions about the estimate of the second-order harmonics (SOH). Subsequently, the HFs are used as examples inside data-driven algorithmic procedures. Furthermore, the optimization of the methodology has become a prominent area of research, alongside the extraction of high-frequency components, which has gained significant attention in recent years [37,38]. In their study, the authors used the Gaussian Process Regression (GPR) model to forecast the SOH of lithium-ion batteries. This was accomplished by extracting three HFs from the voltage, current, and temperature profiles observed throughout the charging and discharging processes. This enabled them to ascertain the projected state of health (SOH) of the battery [39]. In conclusion, this work aims to remove HFs from charging batteries. After that, a Pearson correlation analysis, a Spearman correlation coefficient, and a Kendall rank correlation were used to investigate the relationship between the collected HFs and the capacity of the batteries. In order to assess the SOH of the battery, we will use highly reliable HFs that exhibit a robust capacity correlation. The GWO technique is used to establish the weights and thresholds of the BRNN with the aim of addressing the parameter initialization issue seen in the normal BRNN. The estimate of SOH is conducted by using the GWO-BRNN in order to tackle the aforementioned concerns. The battery dataset provided by NASA is used to validate the efficacy of the proposed GWO-BRNN.

This paper is organized as follows: The data description, extraction of HFs for SOH estimation, and evaluation to select HFs by using correlation analysis have been presented in Section 2. Section 3 describes GWO-BRNN-based SOH estimation incorporating HFs and correlation analysis. The evaluation metrics to assess the effectiveness of the proposed methodology have been discussed in Section 4. The results and analysis of the simulation are presented in Section 5. Section 6 has some last thoughts on the subject.

2. Selection of Health Features for SOH Estimation Based on Correlation Analysis

The most apparent sign of battery deterioration is capacity loss, which is mainly connected to the battery's SOH. SOH is defined by capacity and is provided by the equation below.

$$SOH = \frac{C_{actual}}{C_{nom}} \times 100\% \tag{1}$$

where C_{actual} and C_{nom} stand for real and theoretical capacity, respectively.

2.1. Data Description for SOH Estimation

This study used NASA's B5, B6, B7, and B18 battery records for its investigation and analysis [40,41]. Many researchers in the academic world use the NASA battery dataset as a verification dataset to ensure that their methods are accurate. The accelerated life test platform is responsible for carrying out three distinct battery degeneration tests. This includes the electrochemical impedance experiment, charging, and discharging. Table 1 details the conditions used in the experiments.

Table 1. Selected NASA batteries specifications for analysis.

Battery Number/Specifications		B5	B6	B7	B18
Charging	Constant Current (A)	1.5	1.5	1.5	1.5
	Upper Voltage Limit (V)	4.2	4.2	4.2	4.2
	Cut-off Current (mA)	20	20	20	20
Discharging	Constant Current (A)	2	2	2	2
	Cut-off Voltage (V)	2.7	2.5	2.2	2.5
Operating Conditions	Operating Temperature	Room Temperature	Room Temperature	Room Temperature	Room Temperature
	Initial Capacity (Ah)	1.86	2.04	1.89	1.86
	End of Life (EOL) criteria (Ah)	1.40	1.40	1.40	1.40

The charging process of the B5 battery consists of two distinct stages. Initially, a constant current (CC) mode is employed, where a current of 1.5 A is supplied to the battery until its voltage gradually reaches the charging cut-off voltage. Subsequently, the charging process transitions to the constant voltage (CV) mode, where a current of 0.02 A is maintained to sustain the battery's voltage at the desired level. After twenty minutes of relaxation, the battery is charged. CC mode discharges the battery at 2. A until the cut-off point drains it completely. This process continues until the battery becomes depleted. Figure 1 presents the experimental current and voltage parameters used by NASA. Electrochemical impedance spectroscopy is a technique used to assess the impedance across a frequency range spanning from 0.1 Hz to 5000 Hz.

The battery's capacity exhibits a gradual decline over time as it undergoes charging and discharging cycles, as evidenced by the battery capacity curve observed by NASA. The battery's capacity does not decline continuously, as shown in Figure 2, but rather replenishes on its own. After the charging-discharging cycle is complete, the battery's capacity increases somewhat after being stored for a while. When reactants in a battery concentrate near an electrode, the reaction weakens. Since the battery loses these reactants during storage, its capacity increases throughout the subsequent charging-discharging cycle [42]. In this work, we determine that a battery has reached the junk state when its capacity falls below 70% of its rated capacity, or 1.4 Ah, which is the NASA battery capacity failure criterion.

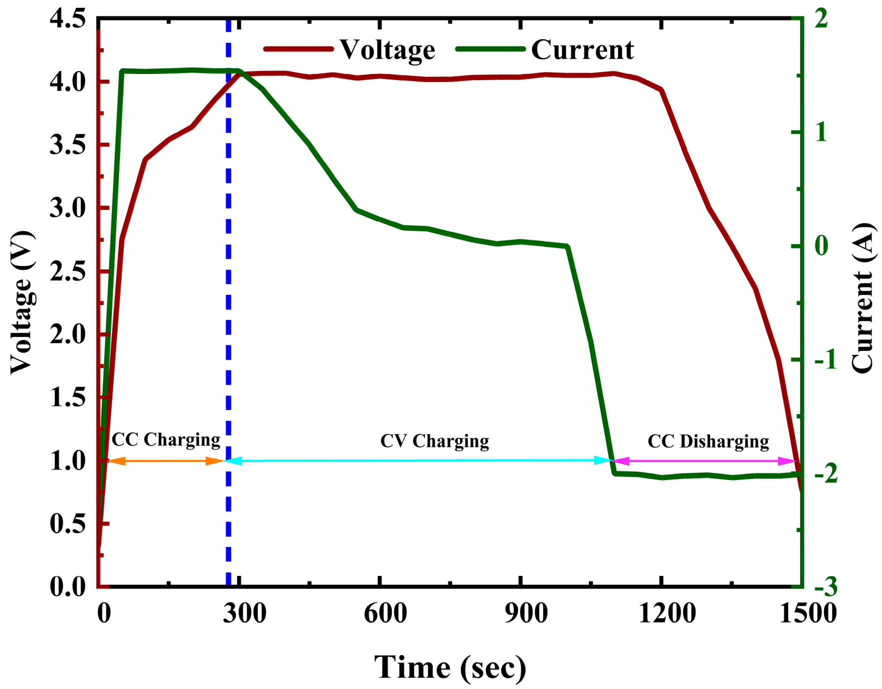

Figure 1. Current/voltage conditions of single charging-discharging of NASA batteries.

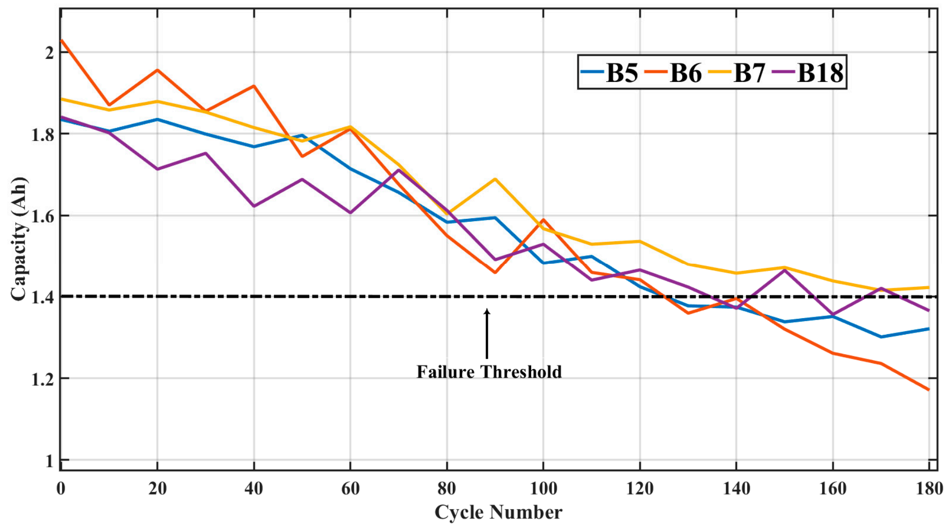

Figure 2. The battery capacity aging curve of NASA batteries of NASA batteries.

The charging current curves exhibit the process of lithium-ion battery degradation over time. The phenomenon of aging, as depicted in Figure 3a,b, can be attributed to the rise in internal ohmic resistance and the gradual loss of capacity resulting from internal physical and chemical mechanisms occurring during both storage and usage. As the quantity of cycles increases, there is a notable fluctuation in the voltage curve observed during the processes of charging and discharging. The data presented in Figure 4a,b demonstrate that the current curves remain consistent irrespective of the number of cycles.

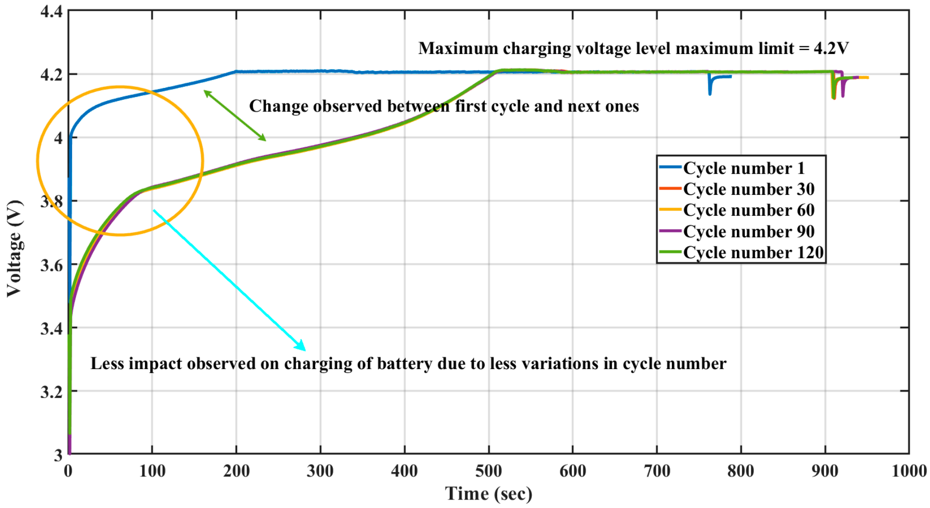

(**a**)

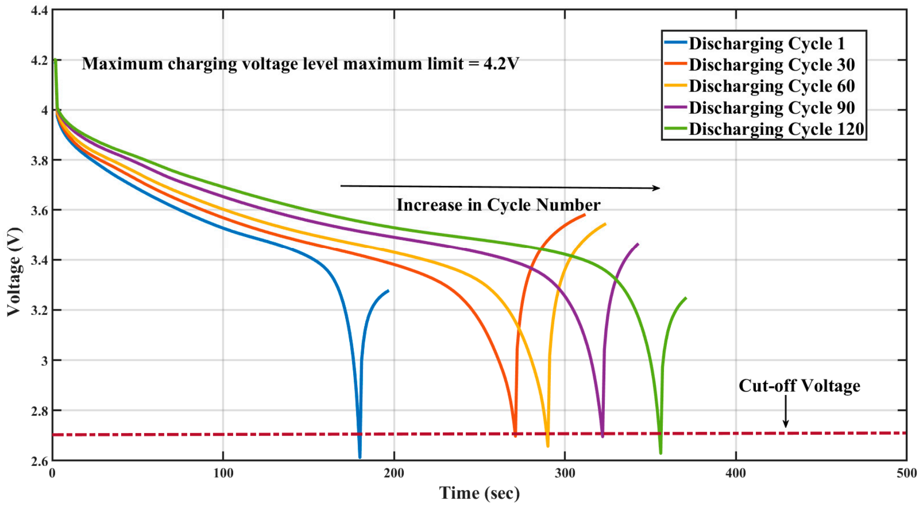

(**b**)

Figure 3. Voltage profiles of NASA B5 battery for different cycles (**a**) Charging (**b**) Discharging.

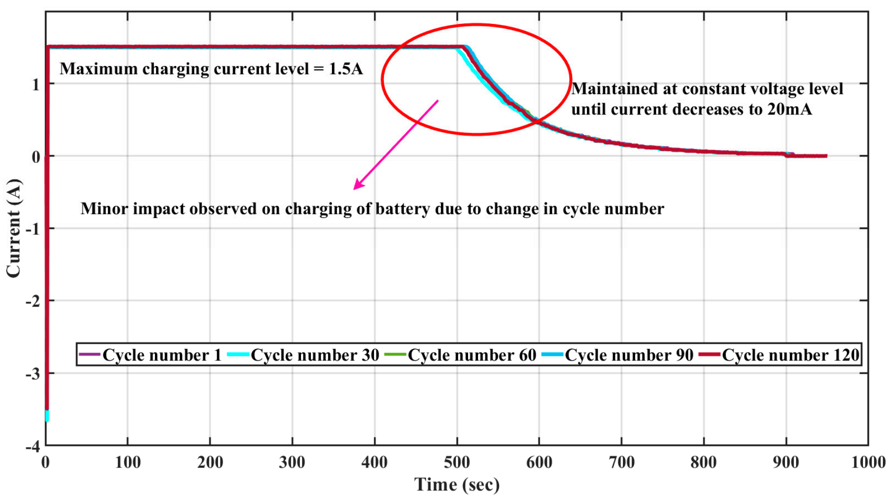

(**a**)

Figure 4. *Cont.*

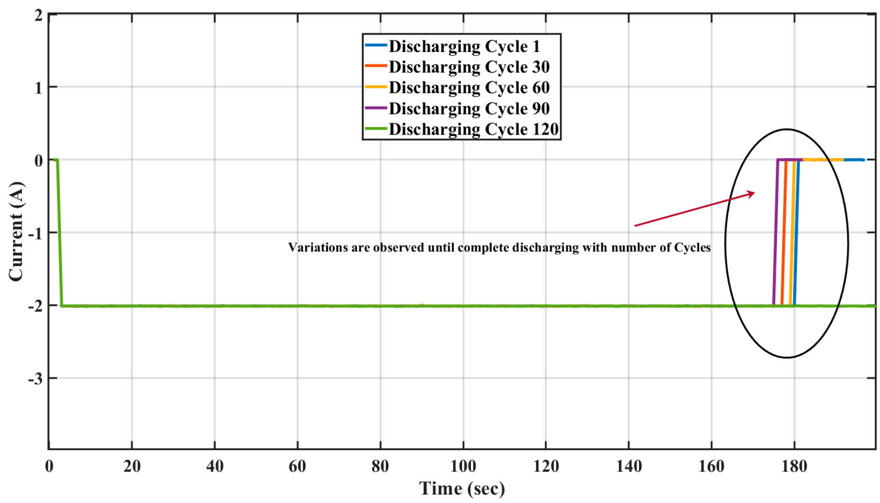

(**b**)

Figure 4. Current profiles of NASA B5 battery for different cycles (**a**) Charging, (**b**) Discharging.

2.2. Extraction of Health Features (HFs) for SOH Estimation

Capacity: The concept of capacity is frequently employed as a key factor in the estimation of battery health. Nevertheless, the determination of battery capacity through direct means is not feasible in practical scenarios due to the intricate nature of the internal reaction within the battery. Additionally, there exists a phenomenon referred to as the self-recovery of the battery's capacity, and the manner in which the battery is discharged is contingent upon the prevailing operating conditions. The direct estimation of SOH using capacity is not feasible due to the complexity of the computational process involved. Consequently, the researchers of this study extract readily quantifiable HFs from the voltage and current profiles observed during the process of battery charging. Battery health is subsequently assessed by identifying HFs that exhibit a strong association with battery capacity, employing diverse correlation coefficients.

The battery's health is reflected in the HFs extracted during the charging-discharging process. That which can be readily tested and monitored online, such as the battery's intrinsic characteristics. The equal discharge voltage duration [43], the incremental capacity curve [44], and the peak temperature of the battery [45] are only a few examples of how current research defines battery HFs. The driver's actions and the surrounding environment significantly impact the power battery's discharge behavior during the operation of an electric vehicle. However, there is a precise procedure for charging batteries. In addition, a battery's capacity to discharge energy is directly related to the quantity of energy it retains during the charging period. Hence, the estimation of SOH and the prediction of RUL can be accomplished by gathering HF data during the charging procedure, facilitating investigations into battery degradation. The charging mode time, also known as the constant current (CC) charging mode time, for lithium-ion batteries used by NASA is denoted as HF_1. Measure the duration required for the voltage to reach the charging cutoff value of 4.2 V during a singular charging cycle. HF_2 represents the voltage at 500 s during CC charging mode. HF_3 denotes the current variation during the first 1000 s of charging in CV mode. HF_4 is the voltage range associated with batteries from 3.7 V to maximum voltage limit of 4.2 V with an interval of 0.1. R1, R2, R3, and R4 represent the ranges of voltages from 3.7 V to 4.2 V with an increment of 0.1. NASA's battery data HFs are extracted as

$$HF_1 = t_{min} = [t_i|V(t_i) = 4.2\ V\ ], t_i = 1, 2, \ldots .T \tag{2}$$

$$HF_2 = V(t = 500\ \mathrm{s}) \tag{3}$$

$$HF_3 = \Delta I_i = 1.5\ A - I\ (t = 1000\ \text{s}) \tag{4}$$

$$HF_4 = \Delta t_i = 3.7 \leq V \leq 4.2\ (\Delta V = 0.1) \tag{5}$$

I represents charging current, V represents charging voltage, and T represents charging time in this equation. The outcomes of HF extraction from NASA batteries are depicted in Figure 5.

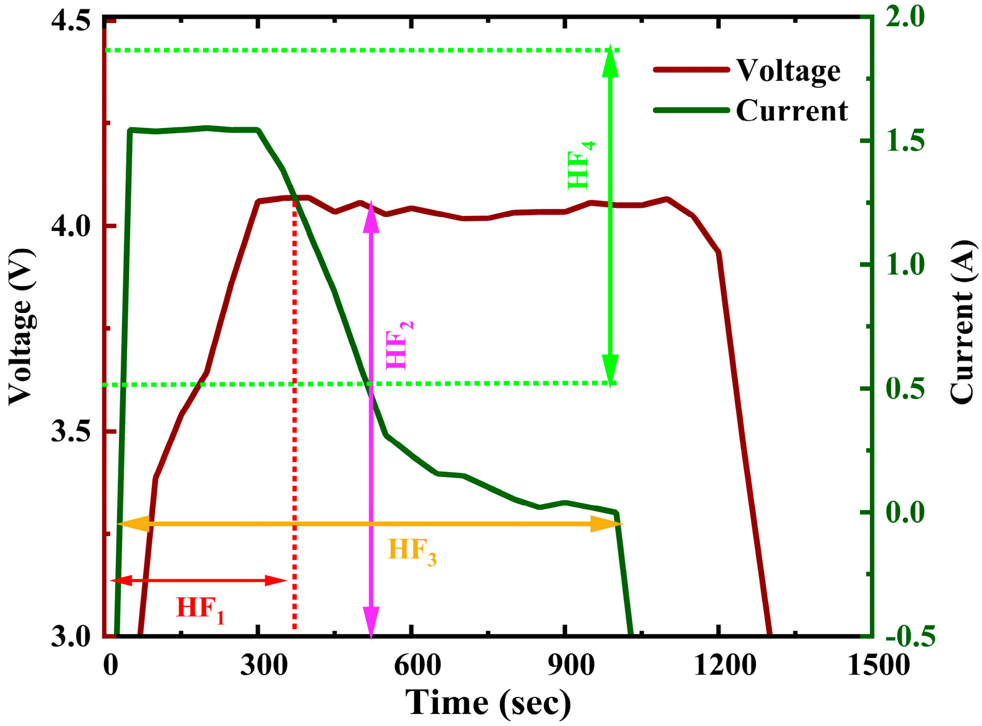

Figure 5. HFs extraction graphic of NASA batteries.

The values of the results will range between 0 and 1. The formula for normalization is as follows:

$$u^* = 1 - \frac{u - u_{min}}{u_{max} - u_{min}} \tag{6}$$

where u represents the data in HFs, u_{min} and u_{max} represent the lowest and maximum values in each HF curve accordingly, and u^* represents the normalized data for HFs.

2.3. Evaluation of HFs for SOH Estimation Based on Correlation Analysis

The Pearson correlation coefficient, often known as PCC, measures the degree to which input parameters and electrical demand rotate linearly. This coefficient may take on values ranging from 0 to 1, inclusive. If the correlation value is between 0.75 and 1, it is considered to have a very strong correlation. If the value is between 0.75 and 0.5, it is considered to have a moderate correlation; if the value is between 0.25 and 1, it is considered to have a weak correlation. "0" implies that there is no connection, but "1" indicates that there is a perfect correlation [36]. Calculating PCC is as follows:

$$\mathtt{C} = \frac{\text{Corr}(U, V)}{T_D(X) \times T_D(V)} = \frac{\sum U_i V_i - \frac{\sum U_i V_i}{m}}{\sqrt{\left(\sum U_i{}^2 - \frac{\sum U_i{}^2}{m}\right)\left(\sum V_i{}^2 - \frac{\sum V_i{}^2}{m}\right)}} \tag{7}$$

The Spearman rank correlation coefficient (ρ) is a non-parametric indicator used to assess the strong monotonic connection between two variables. There are two variables U

$(u_1, u_2, \ldots, u_m)$, and their elements are arranged in ascending order. Equation (8) expresses the Spearman rank correlation coefficient ρ, where $wh(u_i)$ and $wh(v_i)$ denote the new order of u_i and v_i after ascending, respectively.

$$\rho = 1 - \frac{6\sum_{i=1}^{M} g_i^2}{M(M^2-1)}$$

$$g_i = wh(u_i) - wh(v_i) \tag{8}$$

The Kendall rank correlation coefficient (£) is a non-parametric indicator that tests the statistical dependency of two random variables by using the derived value. Any two elements (u_i, v_i) and (u_j, v_j) are regarded as concordant pairs when $u_i > u_j$, $v_i > v_j$ or $u_i < u_j$, $v_i < v_j$; as discordant pairs when $u_i > u_j$, $v_i > v_j$ or $u_i < u_j$, $v_i < v_j$. Equation (9) expresses the Kendall rank correlation coefficient £, where A is the number of concordant pairs, and B is the number of discordant pairs.

$$\text{£} = \frac{A - B}{\frac{1}{2}m(m-1)} \tag{9}$$

The values of C, ρ and £ vary from -1 to +1, with the definition stating that the greater the proximity of the absolute value to 1, the greater the strength of the association. Table 2 presents the results of the calculation of the correlation coefficients. Table 2 shows that all HFs selected for this paper have absolute values of the correlation coefficient with battery capacity greater than 0.6, and most are greater than 0.8. The selected HFs in this study exhibit a robust correlation with battery capacity and will be employed to estimate the SOH.

Table 2. Correlation Analysis Result with battery capacity and different HFs.

Battery	Correlation/HF	$HF_1(t_{min})$	$HF_2(V)$	$HF_3 V(\Delta I_i)$	HF4 (ΔV)				
					R1 (3.7–3.8)	R2 (3.8–3.9)	R3 (3.9–4.0)	R4 (4.0–4.1)	R5 (4.1–4.2)
B5	C	0.847	0.896	0.996	0.817	0.694	0.964	0.924	0.588
	ρ	0.770	0.931	1.060	0.874	0.841	0.891	0.996	0.643
	£	0.743	0.983	0.912	0.982	0.529	0.976	0.987	0.638
B6	C	0.942	0.833	0.976	0.881	0.774	0.989	0.882	0.489
	ρ	0.930	0.719	0.891	0.767	0.680	0.933	0.896	0.401
	£	0.893	0.855	1.000	0.873	0.611	0.919	0.997	0.574
B7	C	0.802	0.860	0.988	0.871	0.692	0.950	0.926	0.580
	ρ	0.939	0.821	0.994	0.782	0.735	0.947	0.783	0.622
	£	0.896	0.761	0.859	0.870	0.743	0.925	0.806	0.372
B18	C	0.947	0.892	1.000	0.744	0.691	0.998	0.833	0.560
	ρ	0.947	0.859	0.982	0.843	0.674	0.975	0.889	0.680
	£	0.799	0.950	0.858	0.714	0.703	0.953	0.959	0.586

The heatmap to show the relationship of battery capacity with HFs extracted for NASA batteries is shown in Figure 6. It can be observed that all batteries HFs used in the analysis have better correlation values greater than 75% for HF_1, HF_2, HF_3, and voltage ranges R1, R3, and R4. However, the voltage ranges R2 and R5 have no strong correlation with battery capacity. They have values of less than 75%, so they are not utilized in the SOH estimation analysis.

Battery	Correlation/HF	HF1	HF2	HF3	HF4				
					R1 (3.7–3.8)	R2 (3.8–3.9)	R3 (3.9–4.0)	R4 (4.0–4.1)	R5 (4.1–4.2)
B5	C	85%	90%	100%	86%	69%	88%	86%	69%
	ϱ	77%	98%	100%	86%	84%	87%	81%	74%
	£	74%	87%	91%	94%	53%	97%	87%	74%
B6	C	94%	86%	98%	72%	77%	88%	92%	59%
	ϱ	93%	75%	89%	77%	68%	89%	84%	50%
	£	89%	91%	100%	78%	61%	91%	97%	67%
B7	C	80%	76%	99%	100%	69%	90%	97%	68%
	ϱ	94%	91%	99%	80%	74%	94%	83%	72%
	£	90%	72%	86%	96%	74%	97%	97%	47%
B18	C	95%	92%	100%	86%	69%	98%	78%	66%
	ϱ	95%	91%	98%	77%	67%	94%	82%	78%
	£	80%	87%	86%	81%	70%	91%	91%	69%

Figure 6. Correlation Analysis for different HFs.

3. GWO-BRNN-Based SOH Estimation Incorporating HFs and Correlation Analysis

In the second stage, we propose to apply optimal BRNN for electric demand forecasting based on selected features. Supervised learning is used for network training in ANN comprising a training set of inputs and outputs in the form $\{i_1,\ s_1\}$, $\{i_2,\ s_2\}$, $\{i_3,\ s_3\}\ldots$, $\{i_m,\ s_m\}$. It has been assumed that outputs are obtained by $Q_m = \sum_{m=1}^{k} i_m r_m$, where w_n is allocated weight for the nth output. Using an activation function, the hidden neurons seek to map input and output for desired results correctly. The initial objective of the training is to minimize the sum of squared errors $F_g = \sum_{m=1}^{k}(s_i - Q_i)$, where Q_i is the neural network response. BRA refers to the steps taken to improve network learning using statistical methods. The network's weights are independent variables. In order to prevent the prediction error associated with over-fitting, BRA uses a set of prior distributions on the model parameters. For better generalization, the predicted output can be expressed as

$$E(r) = ϐ\, F_g + ϭ F_r \tag{10}$$

where F_r represents the total of the squared weights of the network and F_g represents the sum of the squared errors of the network. Both ϐ and ϐ are considered to be objective parameters since they are responsible for determining the amount of error that is associated with the objective function. The primary challenge is to find an optimal set of parameters for the goal function. Following the collection of the data, distribution parameters are determined by the use of statistical methods [46,47]. The probability of a distribution may be expressed in a formula using the Bayesian rule as follows:

$$H(r|G, ϐ,\ ϭ, C) = \frac{H(G|r, ϐ, C)H(r|ϐ, C)}{H(G|ϐ, ϭ, C)} \tag{11}$$

where C represents the neural network architecture, G represents the data collection, and r represents the total number of network weights. $H(w|ϐ, A)$ is the prior distribution that reflects weight knowledge, and $H(G|r, ϐ, C)$ is the likelihood function that describes the probability of the data happening given the weights r. $H(G|ϐ, ϭ, C)$ is the normalization factor that ensures the overall probability is 1. If the weight distribution and data probability distribution are Gaussian, we can describe the probability densities as

$$\begin{cases} H(r|G, ϐ,\ ϭ, C) = \frac{e^{-(ϭ F_g)}}{Y_g(ϐ)} \\ H(G|ϐ, ϭ, C) = \frac{e^{-(\beta ϐ)}}{Y_r(ϭ)} \end{cases} \tag{12}$$

where $Y_g(\text{б}) = \left(\frac{\pi}{\text{б}}\right)^{M/2}$ and $Y_r(\text{ϐ}) = \left(\frac{\pi}{\text{б}}\right)^{m/2}$ with M denoting the number of input-target pairings and m denoting the total number of network weights. Equation (11) is transformed by using the values of these probabilities.

$$H(r|G,\text{ϐ},\ \text{б},C) = \frac{\left(\frac{1}{Y_g(\text{б})}\right)\left(\frac{1}{Y_g(\text{ϐ})}\right)e^{(-(\text{ϐ}F_g+\text{б}F_r\ ))}}{H(G|\text{ϐ},\text{б},C)} = \frac{1}{Y_E(\text{б},\text{ϐ})}e^{(-F(r))} \tag{13}$$

The best weights in this BRA framework should maximize the posterior probability $H(r|G,\text{ϐ},\ \text{б},C)$. Maximizing posterior probability is the same as minimizing the regularized objective function $E(r)$. If a uniform prior density $H(r|\text{ϐ},C)$ is assumed for regularization parameters β and ϐ and, then maximization of the likelihood function $H(G|r,\text{ϐ},C)$ yields the best posterior. The normalization factor for Equation (5) is this likelihood function. The normalization factor may be calculated using Equation (11) as follows.

$$\begin{aligned} H(G|\text{ϐ},\text{б},C) &= \frac{H(G|r,\text{ϐ},C)H(r|\text{ϐ},C)}{H(r|G,\text{ϐ},\ \text{б},C)} \\ H(G|\text{ϐ},\text{б},C) &= \frac{\left[\frac{1}{Y_g(\text{б})}e^{-(\text{б}F_g)}\right]\left[\frac{1}{Y_r(\beta)}e^{-(\text{б}F_r)}\right]}{\frac{1}{Y_E(\text{б},\text{ϐ})}e^{(-E(r))}} \\ &= \frac{Y_E(\text{б},\text{ϐ})}{Y_g(\text{б})Y_r(\text{ϐ})}\text{ϐ}\frac{e^{(-\text{б}F_g-\text{б}F_r)}}{e^{(-E(r))}} = \frac{Y_E(\text{б},\text{ϐ})}{Y_g(\text{б})Y_r(\text{ϐ})} \end{aligned} \tag{14}$$

As the values of $Y_g(\text{б})$ and $Y_r(\text{ϐ})$ can be obtained from Equation (14). $Y_E(\text{б},\text{ϐ})$ can be computed by Taylor series expansion. $E(r)$ can be expanded around the minimum point of the posterior density r^{new}, where the gradient is zero. Solving for normalizing constant $Y_E(\text{б},\text{ϐ})$ can be obtained as

$$Y_E \approx (2\pi)^{m}/_{2}\left(det(P)^{-1}\right)^{\frac{1}{2}} e^{(-E(r^{new}))} \tag{15}$$

where P is the Hessian matrix. It can be approximated as $P = L'L$, where L is a Jacobian matrix. If the Levenberg–Marquardt algorithm (LMA) is used to find the minimum value of $E(r)$, then the Gauss–Newton approximation should be utilized in opposition to the Hessian matrix. In LMA, the parameters that are being used at the nth iteration are updated as the iterations go.

$$r^{m+1} = r^m - \left[L^T L + \theta I\right]^{-1} L^T e \tag{16}$$

where θ is the LMA factor that may be changed at each iteration, as described in [48]. By plugging these numbers into Equation (14), and then solving for the lowest point, we can determine the best values for б and ϐ . The optimum values of б and ϐ may be calculated by taking the derivative with respect to each log of Equation (14) and setting them equal to zero as

$$\text{ϐ}^{new} = \frac{\sigma}{2F_r(r^{new})} \tag{17}$$

$$\gamma^{new} = \frac{n-\sigma}{2F_g(r^{new})} \tag{18}$$

$$\sigma = M - 2\text{ϐ}^{new} trace^{-1}P^* \quad 0 \le \sigma \le M \tag{19}$$

where σ is the number of effective parameters which is a measurement of how many parameters in the network are effectively employed in order to reduce the error function.

Wolves of the grey kind often congregate in packs of 5–12 individuals, with four distinct dominance levels (alpha, beta, delta, and omega). When it comes to hunting, sleeping, and waking up, the alpha grey wolf calls the shots [49]. Pack leaders are not usually the strongest. Betas are second-in-command. They advise alpha wolves. Deltas perform surveillance, protection, hunting, and caregiving. Betas precede deltas. Omega's reign lasted. They eat last. Grey wolves ritually hunt. Their hunting phases are [50] (1) Approaching the prey. (2) Circling and pestering the victim to cease moving. (3) Predation. The following equations explain the hunting process if the prey is up:

$$\vec{J} = 2\vec{j} \cdot \vec{i}_1 - \vec{j}, \tag{20}$$

$$\vec{K} = 2 \cdot \vec{i}_2, \tag{21}$$

$$\vec{L} = \left| \vec{K} \cdot \vec{U}_p(s) - \vec{U}(s) \right. \tag{22}$$

$$\vec{U}(s+1) = \vec{U}_p(s) - \vec{J} \cdot \vec{L} \tag{23}$$

where J and K are coefficient vectors computed using the [0, 1] range random vectors, U (s) is the position vector of the hunting wolf, and U (s + 1) is its updated location in the s + 1 iteration. i_1 and i_2 are components of a vector that decrease from 2 to 0 over the iterations of the method. s is the current iteration. Grey wolves optimize cost function values by ranking them. To mimic the grey wolf social hierarchy, GWO calls the top, second, and third solutions alpha, beta, and delta. Omegas follow alphas, betas, and deltas. We assume the top three wolves know where the prey is in the search space since we do not know where the prey is. Alpha, beta, and delta drive GWO searching. GWO replaces the prey's position with alpha, beta, and delta and updates the remaining wolves' locations in Equations (20)–(23). The updated rules are as follows [51,52].

$$\begin{aligned} \vec{L}_\alpha &= \left| \vec{K}_1 \cdot \vec{U}_a \right|, \\ \vec{L}_\beta &= \left| \vec{K}_2 \cdot \vec{U}_\beta - \vec{U} \right|, \\ \vec{L}_\gamma &= \left| \vec{K}_3 \cdot \vec{U}_\gamma - \vec{U} \right|, \end{aligned} \tag{24}$$

$$\begin{aligned} \vec{U}_1 &= \vec{U}_\alpha - \vec{J}_1 \cdot (\vec{L}_\alpha), \\ \vec{U}_2 &= \vec{U}_\beta - \vec{J}_2 \cdot \left(\vec{L}_\beta\right), \\ \vec{U}_3 &= \vec{U}_\gamma - \vec{J}_3 \cdot \left(\vec{L}_\gamma\right), \end{aligned} \tag{25}$$

$$\vec{U}(s+1) = \frac{\vec{U}_1 + \vec{U}_2 + \vec{U}_3}{3} \tag{26}$$

where Equation (20) calculates J_1, J_2, and J_3, while Equation (21) calculates K_1, K_2, and K_3. Omega is at U (s + 1). During each iteration, the GWO analyzes the cost of all possible solutions, updates the positions of all omega wolves using Equations (24)–(26), and names the top three solutions alpha, beta, and delta. It does this by utilizing Equations (24)–(26). Most algorithms have a set number of iterations. Omega, a two-dimensional search agent, moves to match alpha, beta, and delta. The alpha, beta, and delta wolves estimate the prey's location, while the rest of the pack randomly (and closely) update their position around it. Wolf position vectors describe neural network weights and biases in GWO ANN. Its dimension matches the network's weights and biases. Network pre-prediction error costs. After GWO iterations, the trained network's weights and biases are based on the wolf's position vector with the lowest cost (alpha). GWO-BRNN-based SOH estimation is described below.

1. Collect information about the charging and discharging cycles of the battery, as well as its voltage, current, and any other relevant variables.
2. Remove noise, outliers, and irrelevant features. Normalize data to avoid bias.
3. Train BRNN. BRNN processes noisy data and estimates SOH probabilistically. Populate GWO: Start with random grey wolf placements and speeds.
4. Evaluate the fitness of grey wolves: Evaluate the fitness of each GW by using the BRNN model to predict the SOH based on its position.
5. Fitness-rank alpha, beta, and delta wolves. Grey wolf fitness ranks. The GWO algorithm will place other grey wolves.
6. Investigate the conditions that lead to the termination of the process, such as the maximum number of iterations, the convergence of the fitness function, or a predetermined error threshold.
7. Repeat steps 5–8 until termination criteria are met: Repeat steps 5–8 until the termination criteria are met.
8. Select the optimal grey wolves' position: Select the optimal grey wolves' position with the highest fitness value as the predicted SOH.
9. Evaluate the prediction accuracy: Evaluate the prediction accuracy of the hybrid GWO-BRANN model using validation and testing data.
10. Change model hyperparameters such as the number of grey wolves, learning rate, and regularization strength to improve prediction accuracy.
11. Use the trained hybrid GWO-BRNN model to estimate lithium-ion battery SOH in real-world applications.

4. Evaluation Metrics

We use statistical indicators to evaluate the suggested technique's estimation. The percentage absolute error (F_{AE}) has been calculated using Equation (27) to test the suggested method.

$$F_{\mathrm{AE}} = \left| \frac{U_i - V_i}{U_i} \right| \times 100\% \tag{27}$$

where U_i and V_i represent the actual and SOH predictions by using the proposed approach, respectively. The mean absolute error (F_{MAE}), is the average of the absolute difference between the actual value and the estimated value of SOH for M observations. It characterizes how well the suggested approach works, in general, and is used to determine its typical performance. As a relative error measure, the mean absolute percentage error, abbreviated as (F_{MAPE}), is used to contrast an estimated SOH value with an actual one. The square root of the mean square error, denoted by the notation (F_{RMSE}), is a metric that determines how much the estimated value deviates from the actual value. The coefficient of determination, R squared (R^2), with a range of values from zero to one, is used to evaluate models. Calculations are performed on all the metrics as follows [34,36]:

$$F_{\mathrm{MAE}} = \frac{\sum_{i=1}^{M} (U_i - V_i\ )}{M} \tag{28}$$

$$F_{\mathrm{MAPE}} = \frac{1}{M} \sum_{i=1}^{M} \left| \frac{U_i - V_i}{U_i} \right| \times 100\% \tag{29}$$

$$F_{\mathrm{MSE}} = \frac{1}{M} \sum_{i=1}^{M} (U_i - V_i)^2 \tag{30}$$

$$F_{\mathrm{RMSE}} = \sqrt{\frac{1}{M} \sum_{i=1}^{M} (U_i - V_i)^2} \tag{31}$$

$$R^2 = 1 - \frac{\sum_{i=1}^{M} (U_i - V_i)^2}{\sum_{i=1}^{M} (\check{U}_i - V_i)^2} \tag{32}$$

where $\check{U}_i$ is the mean value. In general, if the F_{MAE}, F_{MAPE}, and F_{RMSE} values are less, it indicates that the estimated performance of the approach is better. A greater impact of model fitting is shown by bigger values of the coefficient of determination, R^2. The framework of GWO-BRNN-based SOH estimation incorporating HFs and correlation analysis is given in Figure 7.

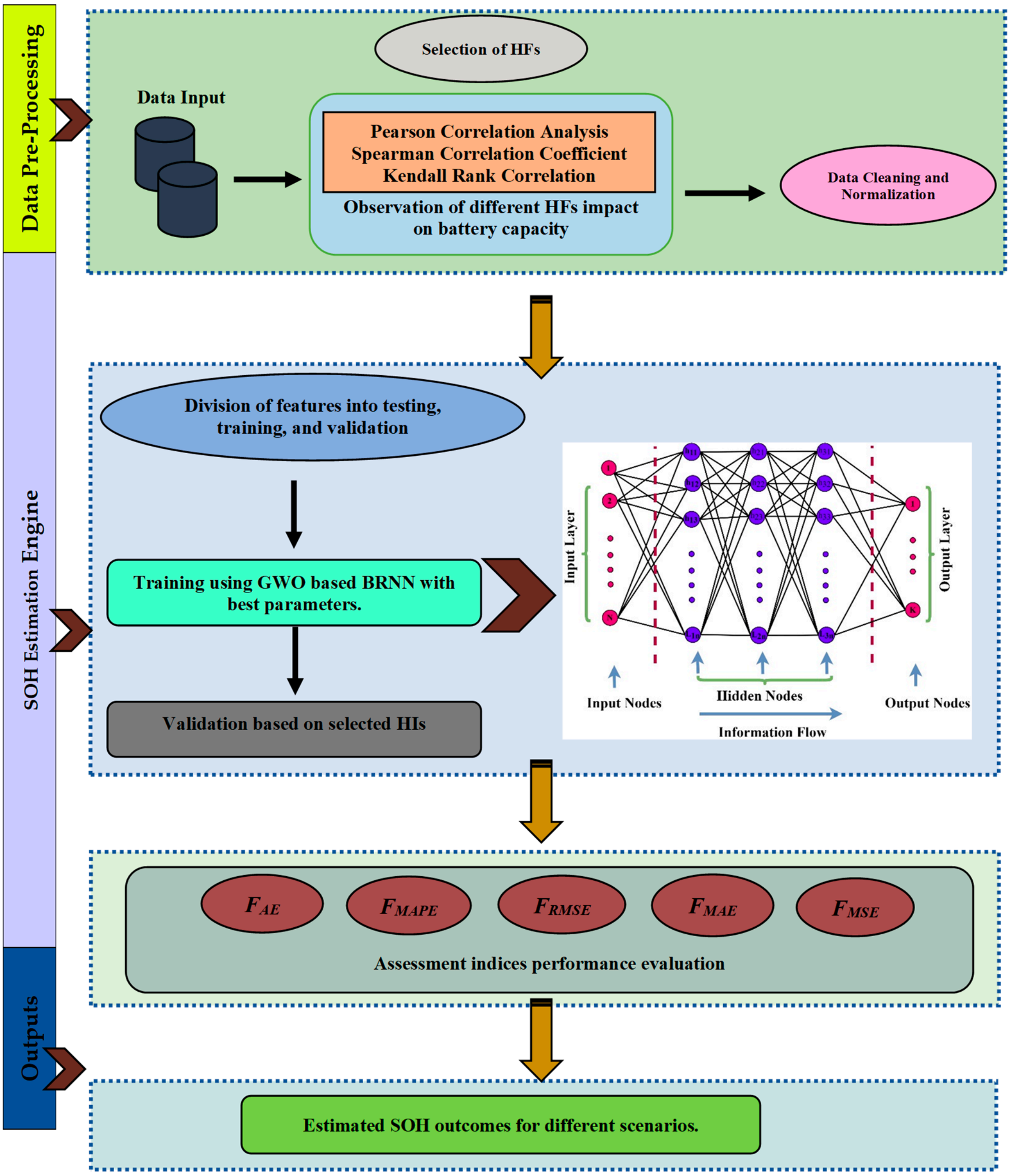

Figure 7. Framework of GWO-BRNN based SOH Estimation incorporating HFs and correlation analysis.

5. Results Analysis and Description

The performance of the proposed GWO-BRNN approach is evaluated using four NASA batteries, namely B5, B6, B7, and B18. This study partitioned the whole dataset into smaller subgroups to facilitate offline training and subsequent online testing. Various sets of sample data are used for offline training of the GWO-BRNN model to examine the SOH of batteries. This study employs 50%, 60%, and 70% of the whole dataset for offline model training, with the remaining dataset allocated for online testing. The proposed approach has also been compared to other methodologies using diverse evaluation indicators. The efficacy of a unique GWO-BRNN methodology has been verified via validation, and the obtained simulation outcomes have been juxtaposed with those of established techniques. The software tool used for this analysis was MATLAB version R2023a, executed on a processor equipped with an Intel (R) Core (TM) i7-10700 CPU operating at 2.90 GHz, and supported by a memory capacity of 16 GB. The experimentation was conducted on a Windows platform.

5.1. SOH Estimation Analysis Based on GWO-BRNN with Different Training Percentages

Based on the GWO-BRNN approach, the estimated SOH for B5, B6, B7, and B18 are shown in Figure 8a–d for a range of training percentages. These figures are shown in order. These are the results of calculations that were carried out using the provided method. These values indicate a wide range of different percentages of training across many different specializations. Looking at Figure 8a–d, it is clear that the recommended approach, which is based on 50%, 60%, and 70% of the training data, has a relatively high level of accuracy. The percentages of training data used demonstrate this. Given the data presented here, it is not difficult to see why. The difference between the three numbers exemplifies this point perfectly. The SOH value estimated by the proposed GWO-BRNN method after training has a high consistency with the SOH reference value, demonstrating the GWO-BRNN technique's effectiveness in SOH estimation. This is demonstrated by the high consistency of the SOH reference value with the estimated SOH value. The table below shows how consistent these values are with one another. This is supported by the fact that the SOH reference value and the projected SOH value are highly congruent with one another, indicating that the statement is true. Given that the SOH value and the SOH reference value share a significant amount of similarity, it is not difficult to reach this conclusion given that the SOH value shares this similarity. In addition to this, the quantity of information utilized during the training process directly impacts the level of precision that can be achieved by the predicted outcomes.

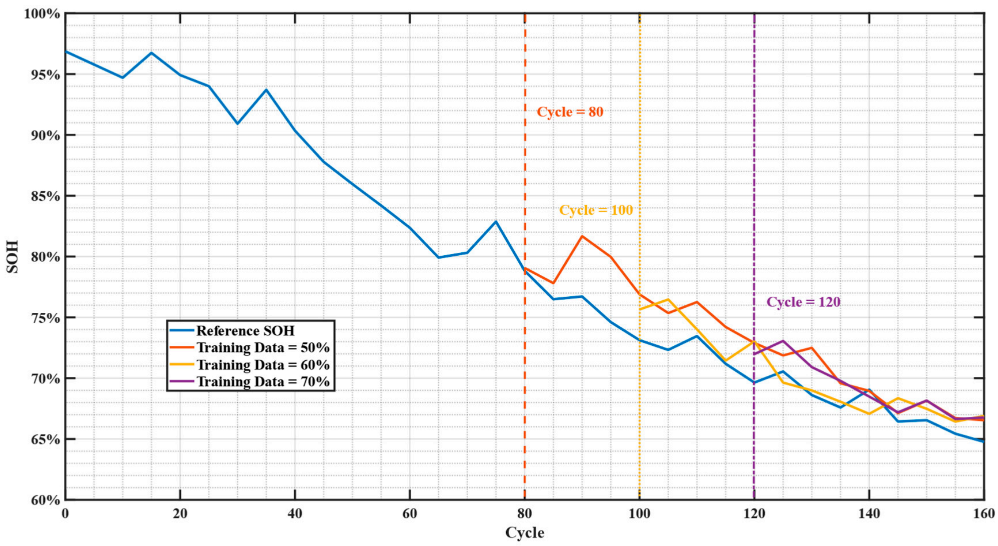

(**a**)

Figure 8. *Cont.*

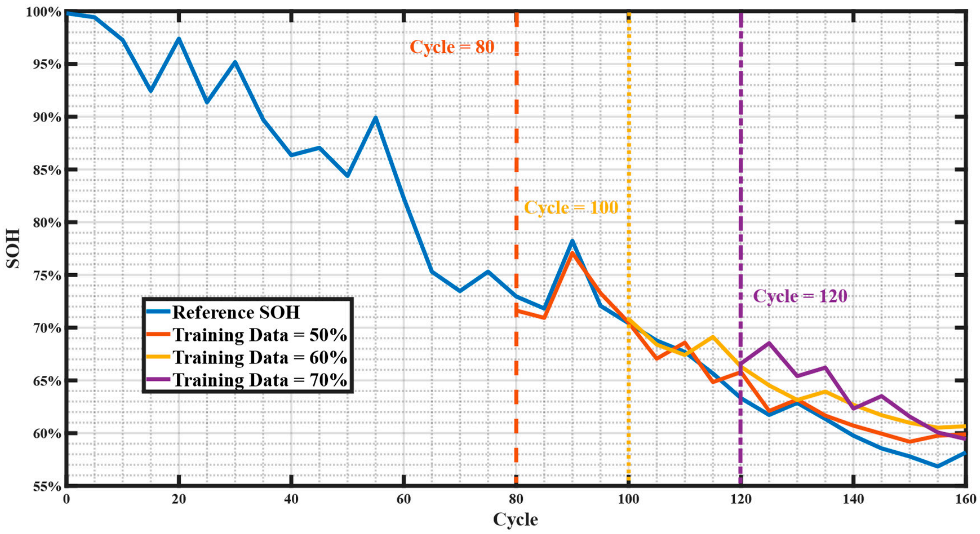

(**b**)

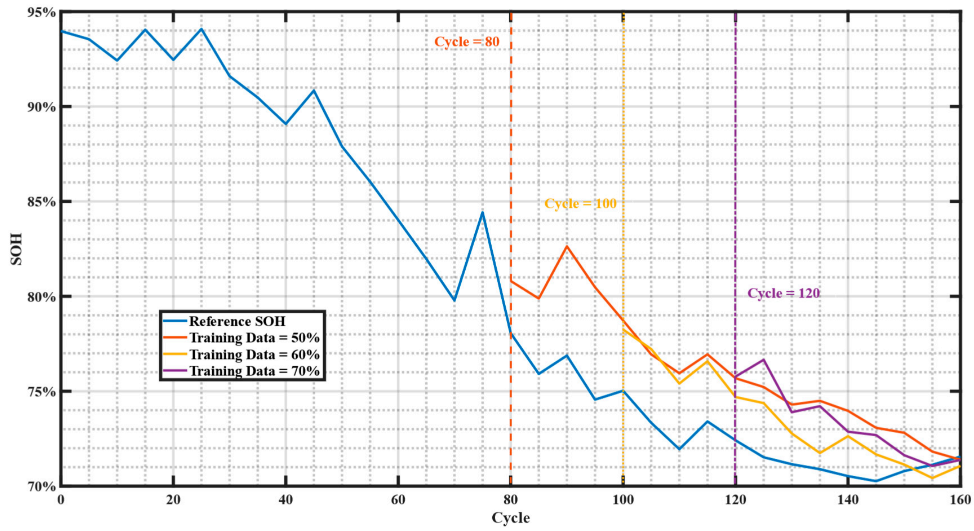

(**c**)

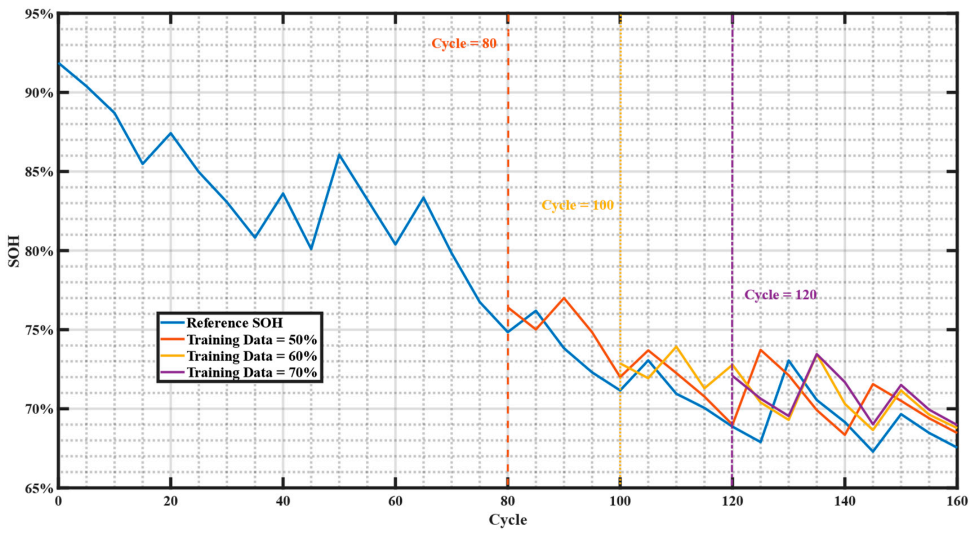

(**d**)

Figure 8. Comparison of SOH by GWO-BRNN for different batteries with different training percentages (**a**) B5 (**b**) B6 (**c**) B7 (**d**) B18.

5.2. Comparison of SOH Estimation Analysis Based on GWO-BRNN with Other Methods

Figure 9 compares the suggested strategy to four other estimate techniques and shows how it can forecast the state of health (SOH) of four different NASA batteries (B5, B6, B7, and B18) with a training percentage of 50%. Additionally, this figure provides a comparison between the recommended technique and the alternative estimation methods. As can be seen in Figure 9a–d, the strategy that has been suggested, which is based on fifty percent of the data that were used for training, produces a high degree of accuracy when applied to B5. This was determined by comparing the results to the original data. In the case of B18, it has been shown that the link between the reference SOH and the anticipated SOH is not as strong as was previously believed to be the case. The SOH value that was estimated by the GWO-BRNN technique after training has a high consistency with the SOH reference value, which shows that the GWO-BRNN approach is successful in SOH estimation. This is shown by the fact that the SOH reference value has a high consistency with the calculated SOH value. This is evident just by looking at the illustrations. This may be seen clearly when one examines the many situations that have been presented. The performance of GA is much lower compared to that of GWO and LMA-ANN, both of which have acquired their findings.

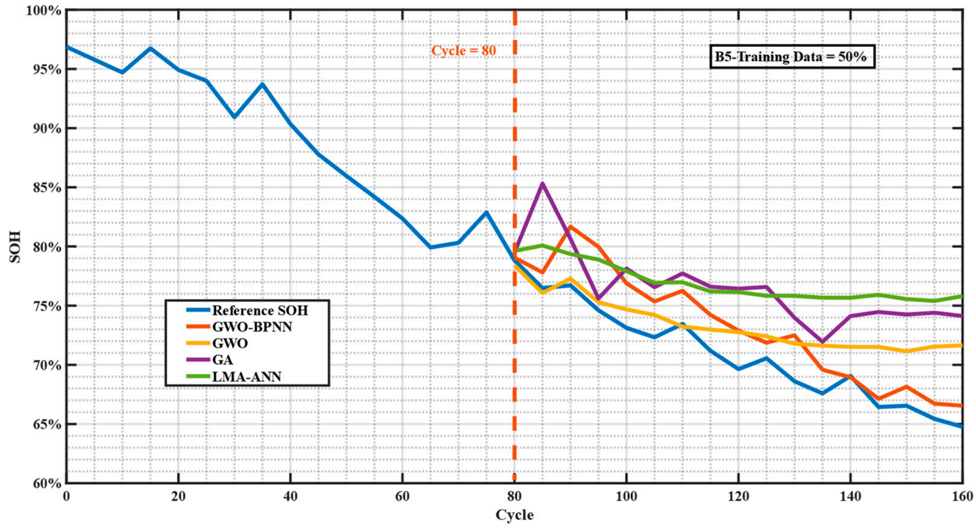

(**a**)

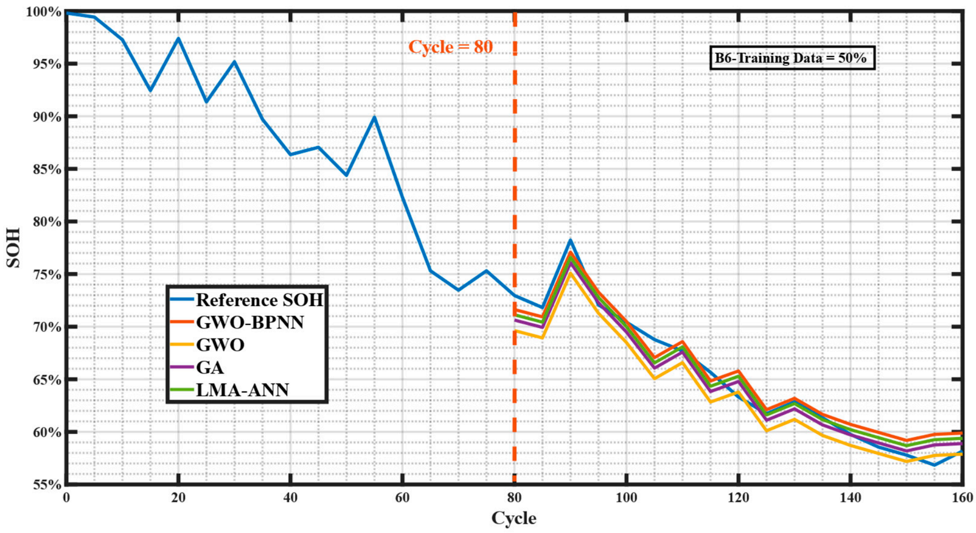

(**b**)

Figure 9. *Cont.*

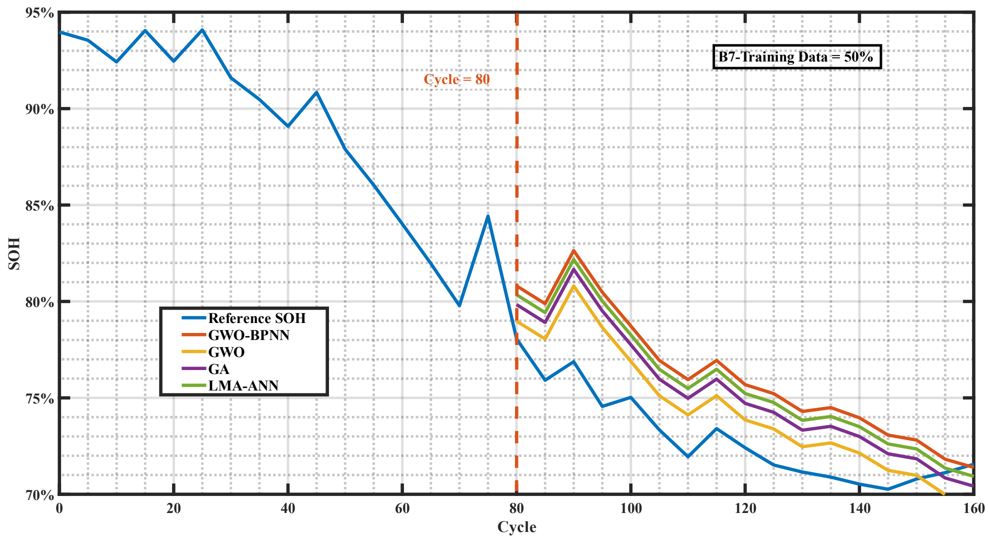

(**c**)

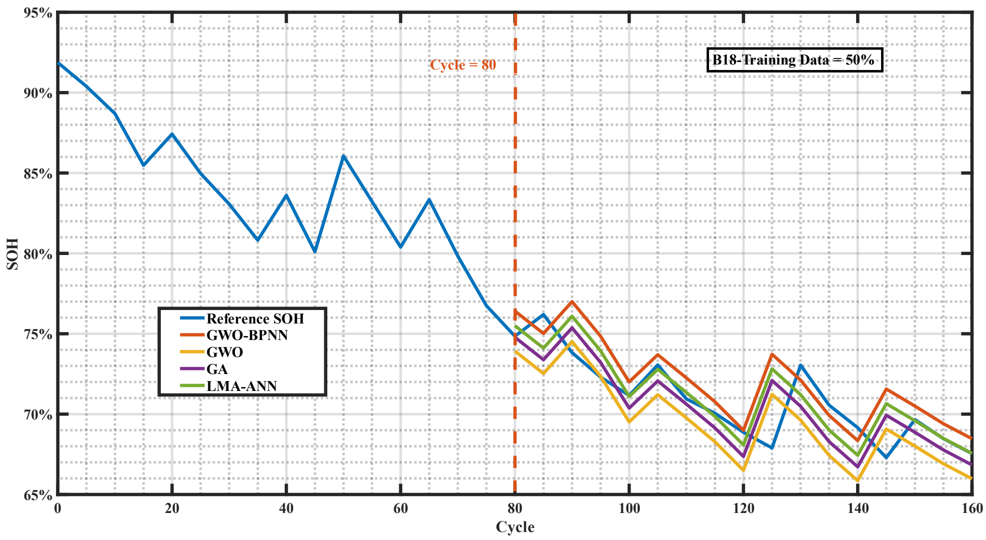

(**d**)

Figure 9. Comparison of SOH for different batteries using different methods with 50% training percentage (**a**) B5 (**b**) B6 (**c**) B7 (**d**) B18.

Figure 10 presents a comparison of the suggested approach to various approaches that are currently in use, as well as an estimate of the SOH for four different NASA batteries (B5, B6, B7, and B18) that were evaluated using the method. The amount of time that will be devoted to training has been determined to be seventy percent of the total available time. In comparison to the method that is only based on half of the training data, the recommended strategy provides excellent accuracy for all of the batteries. This is because it is based on sixty percent of the training data. Figure 10a–d provides further information on this topic. Below is a table that presents the results of a comparison between the accuracy attained by the proposed strategy using 60% of the training data and the technique employing 50% of the training data.

Figure 11 illustrates the State of Health (SOH) estimates for four different types of NASA batteries, namely B5, B6, B7, and B18. The calculations were obtained using a training percentage of 70% and the suggested technique. The figure also includes a comparison of these estimations with other methods. The excellent accuracy of the suggested technique for B5 is shown in Figure 11a–d, where it is seen that the approach is based on 70% of the training data that are available. In comparison to B6, it has been observed that the accuracy of the B7 SOH reference and anticipated SOH levels is somewhat lower. In contrast, the correlation between the projected and actual state of health (SOH) values for B18 has been shown to be the weakest. The observed correlation between the SOH value estimated by the GWO-BRNN technique upon training and the reference SOH value indicates the effectiveness of the GWO-BRNN methodology for estimating SOH. The provided examples serve as illustrations of this concept. When comparing GA to LMA-ANN, it is evident that LMA-ANN exhibits superior performance. When comparing GWO to GA, LMA-ANN, and the projected GWO-BRNN, it can be seen that GWO exhibits the lowest level of performance.

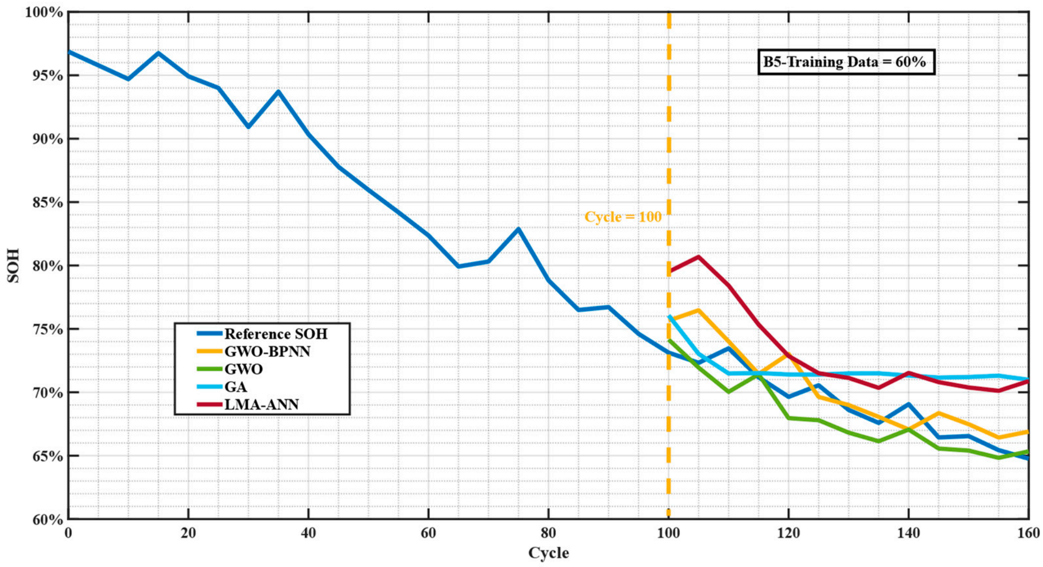

(**a**)

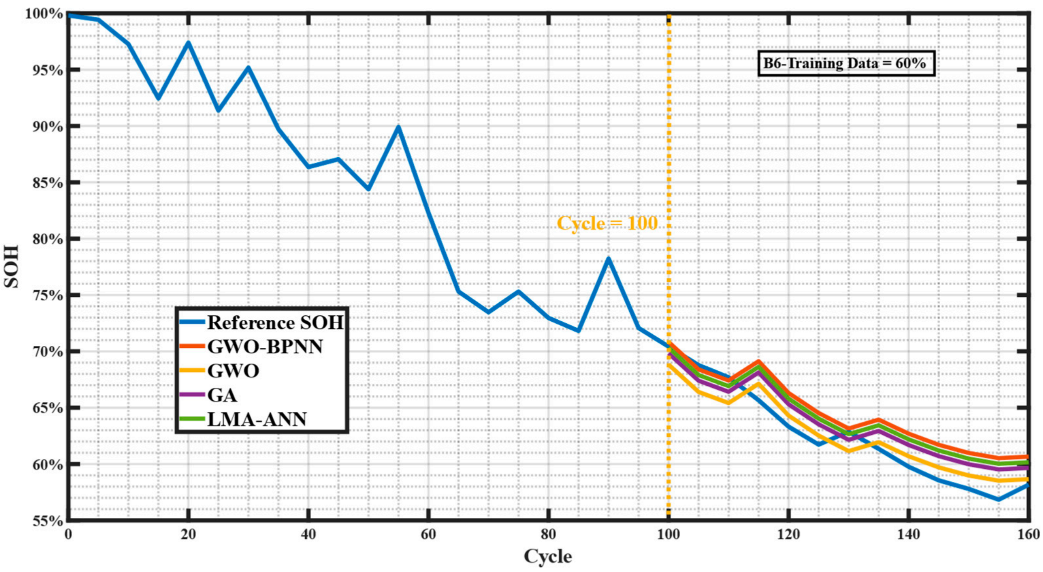

(**b**)

Figure 10. *Cont.*

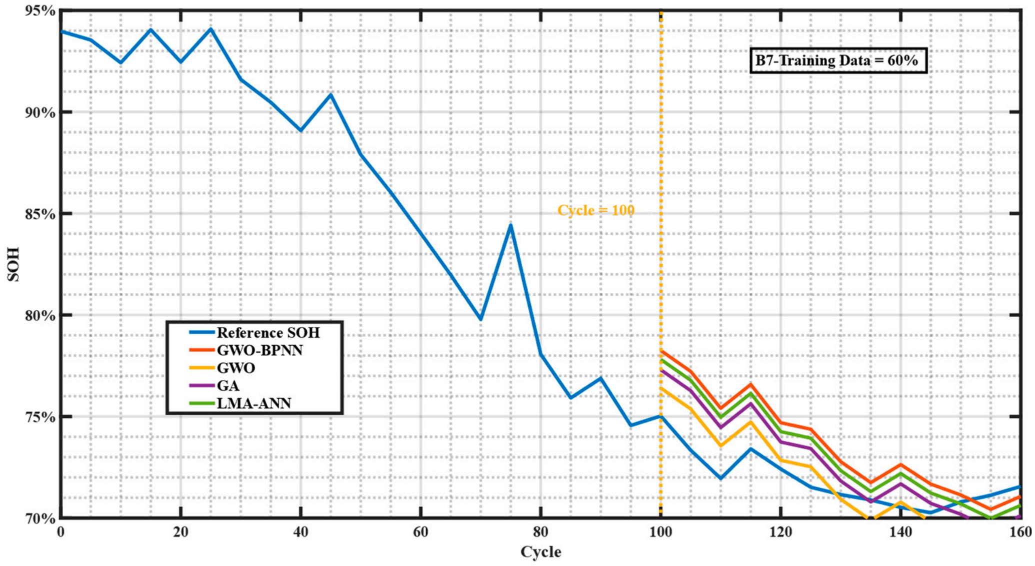

(**c**)

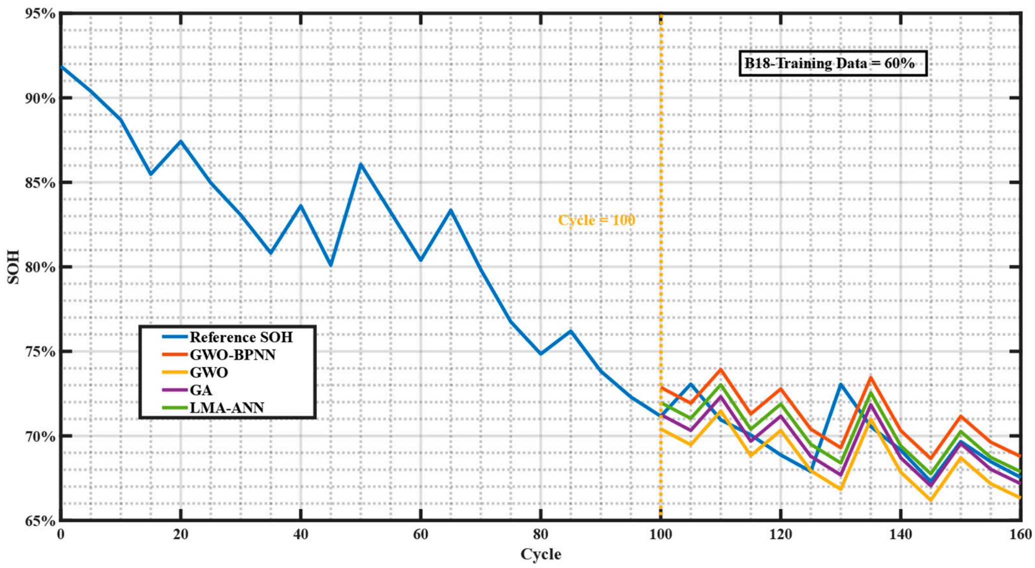

(**d**)

Figure 10. Comparison of SOH for different batteries using different methods with with 60% training percentage (**a**) B5 (**b**) B6 (**c**) B7 (**d**) B18.

In addition, the purpose of this investigation is to evaluate the anticipated state of health (SOH) for batteries by using a variety of algorithms that have been trained on varying percentages of data and taking into account a variety of performance assessment markers. According to the findings, B5 has the lowest values for MAE, RMSE, and MAPE, while also having a larger value for R square. When compared to B7 and B6, respectively, the value of B18 is much greater. Concerning the training percentages, it can be seen that the predicted SOH exhibits the lowest values when the training percentage is set at 70%, as opposed to 60% and 50%, respectively. This is because 70% of the total available time is spent in training. In addition, a thorough examination was carried out to compare and contrast the performance evaluation metrics of the proposed GWO-BRNN with those of the LMA-ANN, GWO, and GA. According to the findings, the GWO-BRNN performs far better than the other approaches, displaying the lowest values across a variety of measures. In addition, the heat map depiction of the SOH forecast is shown for batteries B5, B6, B7, and B18 in Figure 12 and Table 3, which may be found here. The heat map shows the results of using different strategies and training percentages (50, 60, and 70 percent), respectively, in terms of a variety of performance evaluation criteria. According to the findings, the GWO-BRNN model exhibits greater performance in the context of the B5 battery when it is trained using a percentage of 70%. The discrepancy in the accuracy of State of Health (SOH) predictions for B7 batteries, in comparison to batteries with different percentages, can be attributed to variations in charging and discharging behavior, as well as the internal chemistry of the battery. These variations may arise from differences in the internal design characteristics of the battery.

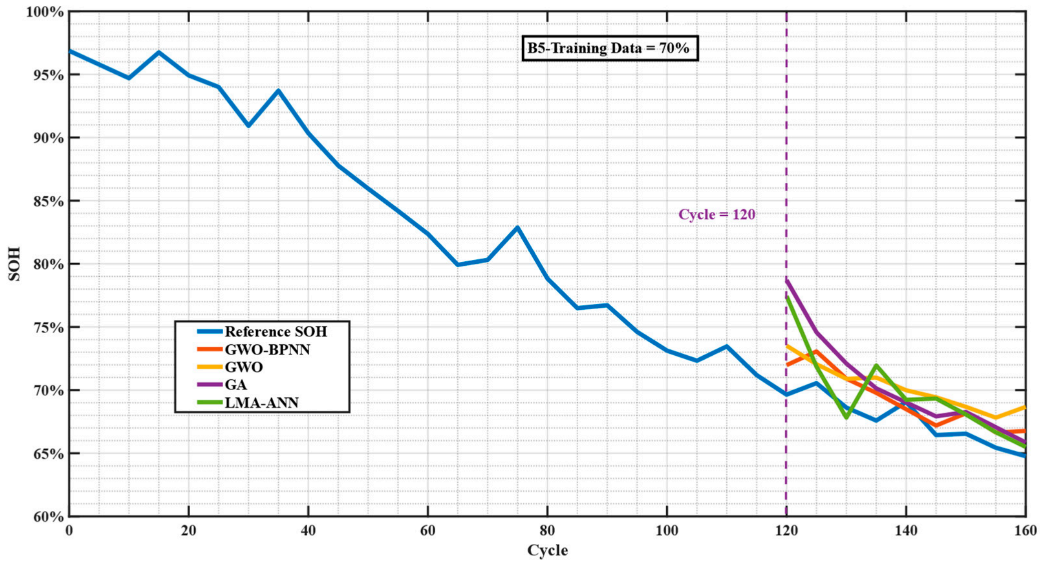

(**a**)

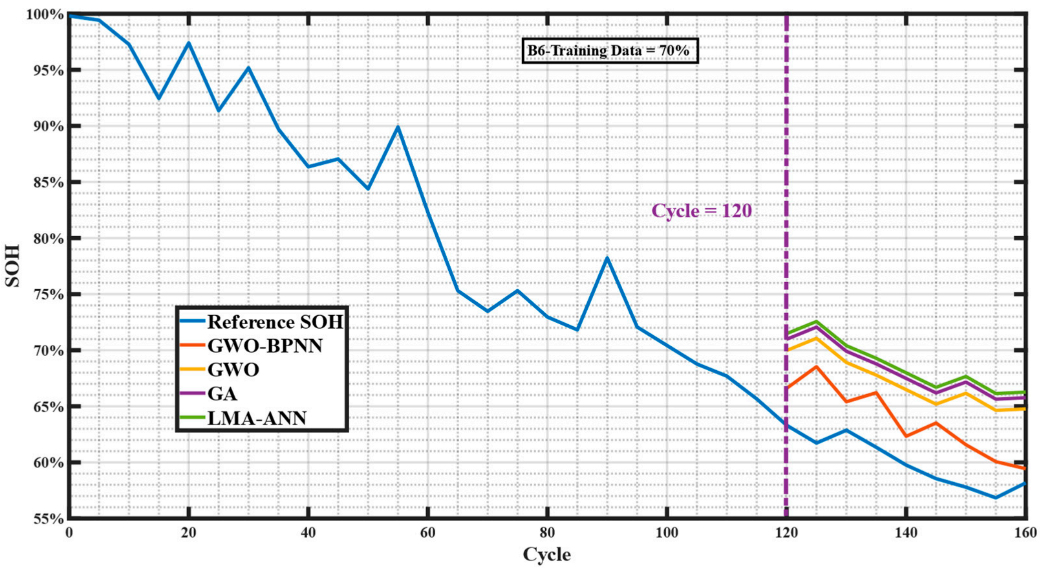

(**b**)

Figure 11. *Cont.*

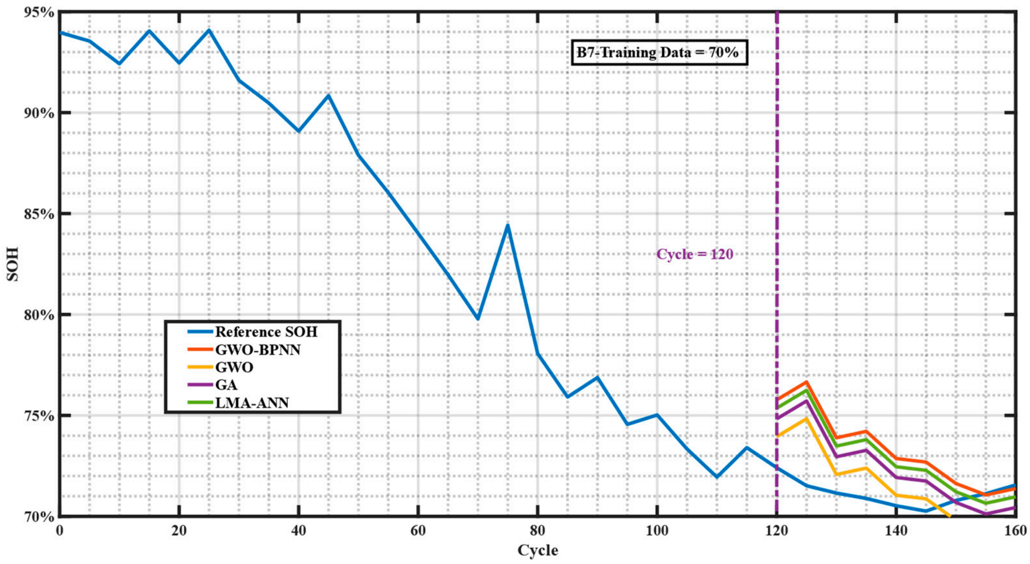

(**c**)

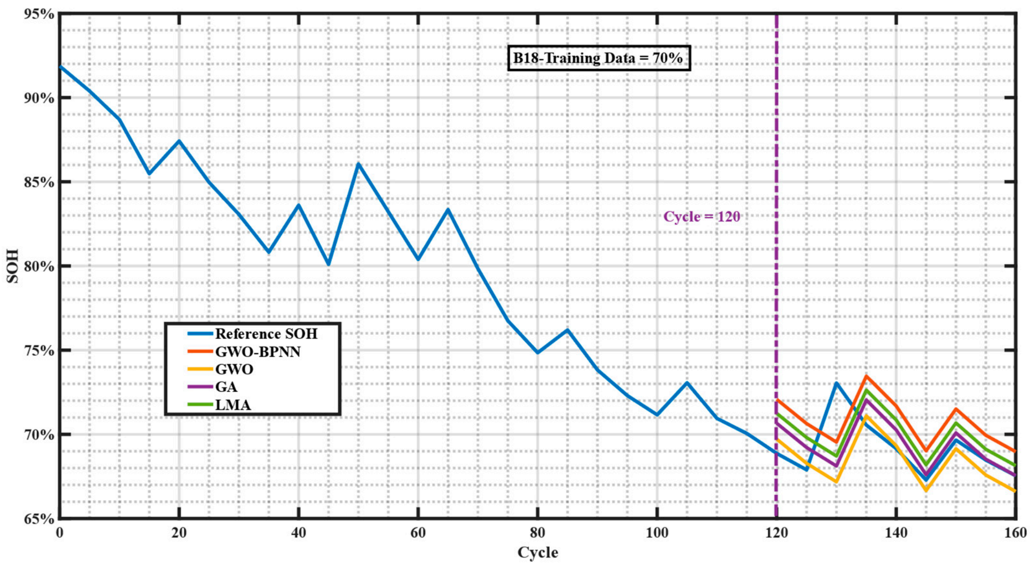

(**d**)

Figure 11. Comparison of SOH by GWO-BRNN for different batteries with other methods with 70% training percentage (**a**) B5 (**b**) B6 (**c**) B7 (**d**) B18.

Table 3. Comparison of SOH for batteries with different approaches and have different training %ages in terms of different performance evaluation metrics.

Training %ages	Method	B5				B6				B7				B18			
		MAE (%)	RMSE (%)	MAPE (%)	R-Square	MAE (%)	RMSE (%)	MAPE (%)	R-Square	MAE (%)	RMSE (%)	MAPE (%)	R-Square	MAE (%)	RMSE (%)	MAPE (%)	R-Square
50	GWO-BRNN	0.379	0.458	0.518	0.995	0.772	0.709	1.197	0.998	0.429	0.568	0.759	0.999	0.927	0.976	1.297	0.994
	GWO	7.563	7.972	3.002	0.949	7.996	8.295	2.898	0.848	7.613	8.052	2.345	0.908	8.475	8.801	2.958	0.822
	GA	3.403	4.002	4.997	0.827	5.420	5.948	7.354	0.857	3.453	5.047	5.998	0.826	5.434	6.072	7.699	0.925
	LM-ANN	2.840	3.382	3.499	0.796	3.624	3.893	5.736	0.784	2.890	3.549	4.943	0.795	4.756	4.179	6.760	0.752
60	GWO-BRNN	0.378	0.409	0.490	0.995	0.749	0.695	1.146	0.998	0.419	0.540	1.048	0.999	0.927	0.942	1.221	0.995
	GWO	5.133	2.479	2.070	0.980	7.403	1.787	2.165	0.860	6.183	3.120	1.837	0.915	7.828	2.050	2.590	0.828

Table 3. *Cont.*

Training %ages	Method	B5				B6				B7				B18			
		MAE (%)	RMSE (%)	MAPE (%)	R-Square	MAE (%)	RMSE (%)	MAPE (%)	R-Square	MAE (%)	RMSE (%)	MAPE (%)	R-Square	MAE (%)	RMSE (%)	MAPE (%)	R-Square
60	GA	3.389	4.070	4.051	0.896	2.531	3.660	3.960	0.895	3.439	3.511	3.710	0.895	2.601	2.812	3.717	0.986
	LM-ANN	1.169	3.189	3.087	0.804	2.557	3.065	4.050	0.813	2.219	3.137	3.115	0.803	3.839	3.936	2.615	0.904
70	GWO-BRNN	0.283	0.375	0.417	0.995	0.720	0.687	1.142	0.998	0.333	0.527	1.047	0.999	0.978	0.928	1.213	0.995
	GWO	4.507	1.951	1.201	0.983	5.469	1.767	2.117	0.905	5.557	2.251	1.817	0.927	6.720	1.770	2.500	0.837
	GA	2.739	2.386	4.038	0.898	1.184	2.427	1.789	0.933	2.789	3.108	2.477	0.897	1.729	2.799	2.430	0.996
	LM-ANN	0.950	2.427	1.376	0.935	1.999	2.272	3.076	0.835	2.000	1.426	2.322	0.934	1.247	2.404	1.780	0.916

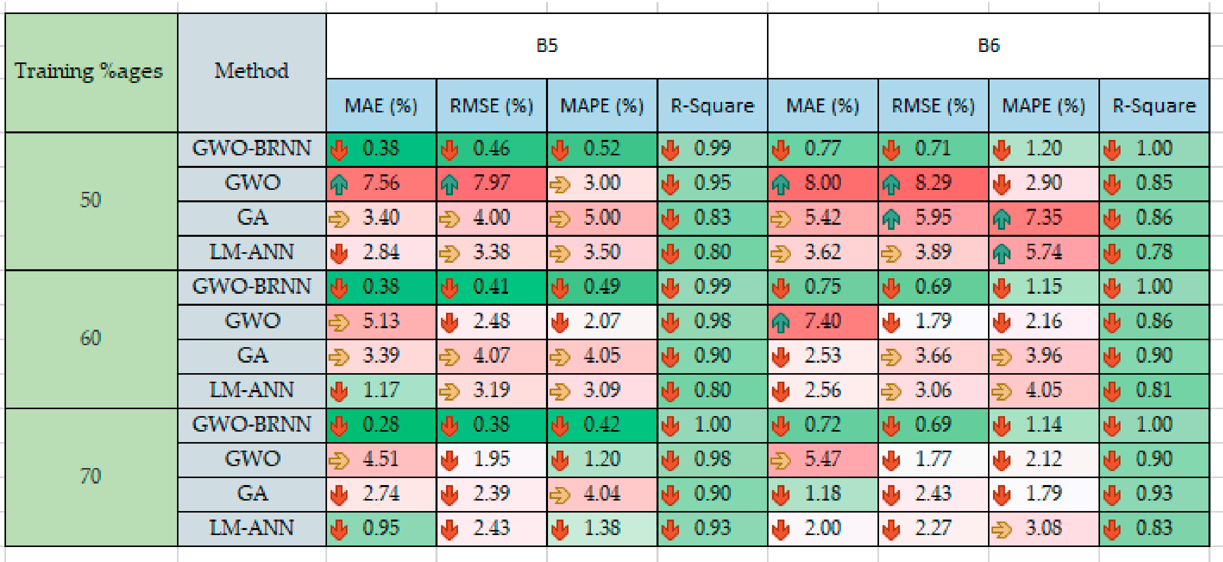

Training %ages	Method	B5				B6			
		MAE (%)	RMSE (%)	MAPE (%)	R-Square	MAE (%)	RMSE (%)	MAPE (%)	R-Square
50	GWO-BRNN	0.38	0.46	0.52	0.99	0.77	0.71	1.20	1.00
	GWO	7.56	7.97	3.00	0.95	8.00	8.29	2.90	0.85
	GA	3.40	4.00	5.00	0.83	5.42	5.95	7.35	0.86
	LM-ANN	2.84	3.38	3.50	0.80	3.62	3.89	5.74	0.78
60	GWO-BRNN	0.38	0.41	0.49	0.99	0.75	0.69	1.15	1.00
	GWO	5.13	2.48	2.07	0.98	7.40	1.79	2.16	0.86
	GA	3.39	4.07	4.05	0.90	2.53	3.66	3.96	0.90
	LM-ANN	1.17	3.19	3.09	0.80	2.56	3.06	4.05	0.81
70	GWO-BRNN	0.28	0.38	0.42	1.00	0.72	0.69	1.14	1.00
	GWO	4.51	1.95	1.20	0.98	5.47	1.77	2.12	0.90
	GA	2.74	2.39	4.04	0.90	1.18	2.43	1.79	0.93
	LM-ANN	0.95	2.43	1.38	0.93	2.00	2.27	3.08	0.83

(**a**)

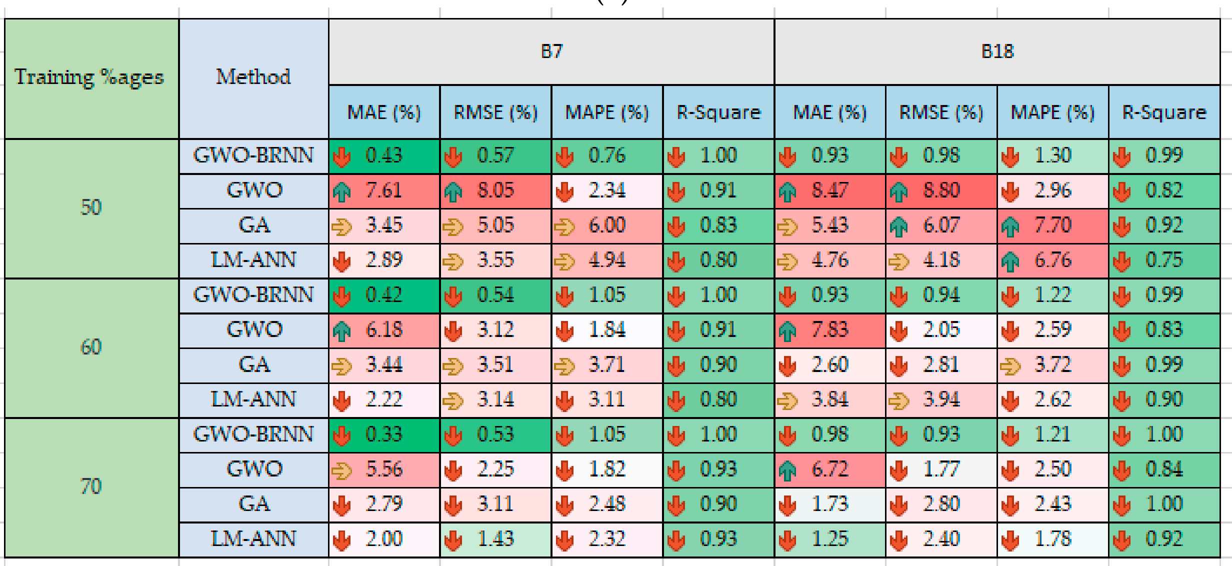

Training %ages	Method	B7				B18			
		MAE (%)	RMSE (%)	MAPE (%)	R-Square	MAE (%)	RMSE (%)	MAPE (%)	R-Square
50	GWO-BRNN	0.43	0.57	0.76	1.00	0.93	0.98	1.30	0.99
	GWO	7.61	8.05	2.34	0.91	8.47	8.80	2.96	0.82
	GA	3.45	5.05	6.00	0.83	5.43	6.07	7.70	0.92
	LM-ANN	2.89	3.55	4.94	0.80	4.76	4.18	6.76	0.75
60	GWO-BRNN	0.42	0.54	1.05	1.00	0.93	0.94	1.22	0.99
	GWO	6.18	3.12	1.84	0.91	7.83	2.05	2.59	0.83
	GA	3.44	3.51	3.71	0.90	2.60	2.81	3.72	0.99
	LM-ANN	2.22	3.14	3.11	0.80	3.84	3.94	2.62	0.90
70	GWO-BRNN	0.33	0.53	1.05	1.00	0.98	0.93	1.21	1.00
	GWO	5.56	2.25	1.82	0.93	6.72	1.77	2.50	0.84
	GA	2.79	3.11	2.48	0.90	1.73	2.80	2.43	1.00
	LM-ANN	2.00	1.43	2.32	0.93	1.25	2.40	1.78	0.92

(**b**)

Figure 12. Heat Map Representation of SOH Estimation for batteries with GWO-BRNN and different approaches with different training %ages (**a**) B5 and B6 (**b**) B7 and B18 in terms of different performance evaluation metrics.

6. Conclusions

In light of the research paper outcomes, an innovative technique called GWO-BRNN has been proposed to determine the state of health (SOH) of a battery by extracting health features (HFs). Since directly measuring capacity is challenging, the SOH has been approximated by utilizing HFs combined with current, voltage, and time. The selection of HFs is based on criteria such as the Pearson correlation coefficient (PCC), the Spearman rank correlation coefficient, and the Kendall rank correlation coefficient. The BRNN algorithm is suitable for use in time series estimation; however, a problem still needs to be solved regarding the selection of appropriate hyperparameters. Consequently, the authors of this work advise that the GWO methodology be utilized to locate the optimal values for the BRNN model's hyperparameters. In contrast to the conventional way, the use of GWO-BRNN has the potential to successfully mitigate the issue of sliding towards local extremes and arrive at the globally optimum solution. This is in contrast to the traditional method, which does not have this capability. In order to obtain better estimate performance, the GWO approach is used in order to fine-tune the BRNN model's hyperparameters and attain optimal values for them.

The SOH estimate is calculated based on the proposed method, and NASA battery datasets are used to carry out the calculation so that the performance of the suggested technique can be checked and evaluated. Using these datasets allows for the achievement of the desired results. According to the findings of the comparison, the presented GWO-BRNN approach has a higher accuracy level when compared to other methods such as LM-ANN, GWO, and GA. These findings were found by examining the similarities and differences between each of these approaches. For all of the batteries, the R-square value of the GWO-BRNN approach is almost equal to 0.99, and the RMSE, MAE, and MAPE values are all less than 1%. Additionally, the R-square value of the GWO-BRNN technique is nearly equal to 0.99. This indicates that the GWO-BRNN method is more accurate than other approaches because of the way it is constructed. The suggested method keeps a respectable estimate performance for the given data set. In conclusion, the proposed methodology has the potential for real-world implementation in the future. Additionally, a training percentage of 70% yields superior results compared to 60% and 50% for the battery datasets. Among B5, B6, B7, and B18, the SOH prediction results for B5 demonstrate higher accuracy than those for other batteries. Although the GWO-BRNN technique developed for evaluating the SOH of lithium-ion batteries has notable benefits, it is crucial to acknowledge possible limits. One notable difficulty pertains to the computational complexity associated with optimization and selection procedures, which may need substantial computer resources. Moreover, the BRNN model's interpretability and the underlying aging process may provide difficulties, given that neural networks are often regarded as opaque models. These constraints need meticulous deliberation in striking a balance between the precision and intricacy of the methodology. However, the technique that has been suggested continues to show potential in the field of EV battery prognostics and health management. This has the potential to greatly contribute to the increased use of environmentally friendly and reliable electric transportation.

Future directions in the context of EVs can concentrate on several key areas. The expansion of the infrastructure for charging, including the installation of fast-charging stations and the incorporation of wireless charging technologies, will allay range anxiety concerns and give EV owners more practical charging options. Moreover, integrating EVs with renewable energy sources and smart grid systems will allow for intelligent charging and vehicle-to-grid (V2G) capabilities. This will allow EVs to serve as flexible energy storage resources and help keep the grid stable. The advancement of autonomous driving technologies and the emergence of shared mobility services will transform the EV landscape, increasing the accessibility, efficiency, and utilization of electric vehicles. Ultimately, ongoing EV manufacturing and design research and development efforts will continue to improve vehicle efficiency, aerodynamics, and lightweight materials, resulting in more energy-efficient and environmentally friendly electric vehicles.

Author Contributions: Conceptualization, M.W.; methodology, M.W.; software, M.W.; validation, M.W.; formal analysis, M.W.; investigation, M.W., J.H., C.-N.W. and C.K.M.L.; resources, M.W.; data curation, M.W.; writing—original draft preparation, M.W.; writing—review and editing, M.W., J.H., C.-N.W. and C.K.M.L.; visualization, supervision, C.K.M.L.; project administration, J.H. and C.-N.W. All authors have read and agreed to the published version of the manuscript.

Funding: This research received no external funding.

Data Availability Statement: Available upon request.

Acknowledgments: The work presented in this article is supported by the Centre for Advances in Reliability and Safety (CAiRS) admitted under AIR@InnoHK Research Cluster.

Conflicts of Interest: The authors declare no conflict of interest.

References

1. Mihet-Popa, L.; Saponara, S. Power converters, electric drives and energy storage systems for electrified transportation and smart grid applications. *Energies* **2021**, *14*, 4142. [CrossRef]
2. Gonzalez, I.; Calderón, A.J.; Folgado, F.J. IoT real time system for monitoring lithium-ion battery long-term operation in microgrids. *J. Energy Storage* **2022**, *51*, 104596. [CrossRef]
3. Waseem, M.; Adnan Khan, M.; Goudarzi, A.; Fahad, S.; Sajjad, I.A.; Siano, P. Incorporation of blockchain technology for different smart grid applications: Architecture, prospects, and challenges. *Energies* **2023**, *16*, 820. [CrossRef]
4. Chen, T.; Jin, Y.; Lv, H.; Yang, A.; Liu, M.; Chen, B.; Xie, Y.; Chen, Q. Applications of Lithium-Ion Batteries in Grid-Scale Energy Storage Systems. *Trans. Tianjin Univ.* **2020**, *26*, 208–217. [CrossRef]
5. Amin, M.A.; Suleman, A.; Iqbal, T.; Aziz, S.; Faiz, M.T.; Zulfiqar, L.; Saleh, A.M. Renewable Energy Maximization for Pelagic Islands Network of Microgrids Through Battery Swapping Using Deep Reinforcement Learning. *IEEE Access* **2023**, *11*, 86196–86213. [CrossRef]
6. Chen, Y. Research on collaborative innovation of key common technologies in new energy vehicle industry based on digital twin technology. *Energy Rep.* **2022**, *8*, 15399–15407. [CrossRef]
7. Çelik, D.; Meral, M.E. Investigation and analysis of effective approaches, opportunities, bottlenecks and future potential capabilities for digitalization of energy systems and sustainable development goals. *Electr. Power Syst. Res.* **2022**, *211*, 108251.
8. Potrykus, S.; Kutt, F.; Nieznański, J.; Fernández Morales, F.J. Advanced Lithium-Ion Battery Model for Power System Performance Analysis. *Energies* **2020**, *13*, 2411. [CrossRef]
9. Goudarzi, A.; Ghayoor, F.; Fahad, S.; Traore, I. A Survey on IoT-Enabled Smart Grids: Emerging, Applications, Challenges, and Outlook. *Energies* **2022**, *15*, 6984. [CrossRef]
10. Hao, W.; Xie, J. Reducing diffusion-induced stress of bilayer electrode system by introducing pre-strain in lithium-ion battery. *J. Electrochem. Energy Convers. Storage* **2021**, *18*, 020909. [CrossRef]
11. Zhou, D.; Wang, B.; Zhu, C.; Zhou, F.; Wu, H. A light-weight feature extractor for lithium-ion battery health prognosis. *Reliab. Eng. Syst. Saf.* **2023**, *237*, 109352. [CrossRef]
12. Yao, L.; Xu, S.; Tang, A.; Zhou, F.; Hou, J.; Xiao, Y.; Fu, Z. A review of lithium-ion battery state of health estimation and prediction methods. *World Electr. Veh. J.* **2021**, *12*, 113. [CrossRef]
13. Gholizadeh, M.; Yazdizadeh, A. Systematic mixed adaptive observer and EKF approach to estimate SOC and SOH of lithium–ion battery. *IET Electr. Syst. Transp.* **2020**, *10*, 135–143. [CrossRef]
14. Bi, Y.; Yin, Y.; Choe, S.-Y. Online state of health and aging parameter estimation using a physics-based life model with a particle filter. *J. Power Sources* **2020**, *476*, 228655. [CrossRef]
15. Khan, M.A.; Saleh, A.M.; Sajjad, I.A. Artificial Intelligence Enabled Demand Response: Prospects and Challenges in Smart Grid Environment. *IEEE Access* **2023**, *11*, 1477–1505.
16. Yang, K.; Zhang, L.; Zhang, Z.; Yu, H.; Wang, W.; Ouyang, M.; Zhang, C.; Sun, Q.; Yan, X.; Yang, S. Battery state of health estimate strategies: From data analysis to end-cloud collaborative framework. *Batteries* **2023**, *9*, 351.
17. Chi, R.; Li, H.; Shen, D.; Hou, Z.; Huang, B. Enhanced P-Type Control: Indirect Adaptive Learning from Set-Point Updates. *IEEE Trans. Autom. Control* **2023**, *68*, 1600–1613. [CrossRef]
18. Wang, Z.; Yuan, C.; Li, X. Lithium Battery State-of-Health Estimation via Differential Thermal Voltammetry with Gaussian Process Regression. *IEEE Trans. Transp. Electrif.* **2021**, *7*, 16–25. [CrossRef]
19. Grisales-Noreña, L.F.; Montoya, O.D.; Perea-Moreno, A.-J. Optimal Integration of Battery Systems in Grid-Connected Networks for Reducing Energy Losses and CO2 Emissions. *Mathematics* **2023**, *11*, 1604. [CrossRef]
20. Sun, C.; Qu, A.; Zhang, J.; Shi, Q.; Jia, Z. Remaining Useful Life Prediction for Lithium-Ion Batteries Based on Improved Variational Mode Decomposition and Machine Learning Algorithm. *Energies* **2023**, *16*, 313. [CrossRef]
21. Zhang, H.; Liu, Y.; Yang, X. An efficient ADI difference scheme for the nonlocal evolution problem in three-dimensional space. *J. Appl. Math. Comput.* **2023**, *69*, 651–674. [CrossRef]

22. Chen, S.; Li, J.; Jiang, C.; Xiao, W. Optimal Energy-Storage Configuration for Microgrids Based on SOH Estimation and Deep Q-Network. *Entropy* **2022**, *24*, 630. [CrossRef]
23. Driscoll, L.; de la Torre, S.; Gomez-Ruiz, J.A. Feature-based lithium-ion battery state of health estimation with artificial neural networks. *J. Energy Storage* **2022**, *50*, 104584. [CrossRef]
24. Chen, Z.; Sun, M.; Shu, X.; Xiao, R.; Shen, J. Online State of Health Estimation for Lithium-Ion Batteries Based on Support Vector Machine. *Appl. Sci.* **2018**, *8*, 925. [CrossRef]
25. Yang, D.; Zhang, X.; Pan, R.; Wang, Y.; Chen, Z. A novel Gaussian process regression model for state-of-health estimation of lithium-ion battery using charging curve. *J. Power Sources* **2018**, *384*, 387–395. [CrossRef]
26. Liu, K.; Li, Y.; Hu, X.; Lucu, M.; Widanage, W.D. Gaussian Process Regression with Automatic Relevance Determination Kernel for Calendar Aging Prediction of Lithium-Ion Batteries. *IEEE Trans. Ind. Inform.* **2020**, *16*, 3767–3777. [CrossRef]
27. Zhang, L.; Yin, Q.; Zhu, W.; Lyu, L.; Jiang, L.; Koh, L.H.; Cai, G. Research on the orderly charging and discharging mechanism of electric vehicles considering travel characteristics and carbon quota. *IEEE Trans. Transp. Electrif.* **2023**, 1. [CrossRef]
28. Su, X.; Sun, B.; Wang, J.; Zhang, W.; Ma, S.; He, X.; Ruan, H. Fast capacity estimation for lithium-ion battery based on online identification of low-frequency electrochemical impedance spectroscopy and Gaussian process regression. *Appl. Energy* **2022**, *322*, 119516. [CrossRef]
29. Khumprom, P.; Yodo, N. A data-driven predictive prognostic model for lithium-ion batteries based on a deep learning algorithm. *Energies* **2019**, *12*, 660. [CrossRef]
30. Zhao, H.; Chen, Z.; Shu, X.; Shen, J.; Lei, Z.; Zhang, Y. State of health estimation for lithium-ion batteries based on hybrid attention and deep learning. *Reliab. Eng. Syst. Saf.* **2023**, *232*, 109066. [CrossRef]
31. He, K.; Zhang, C.; He, Q.; Wu, Q.; Jackson, L.; Mao, L. Effectiveness of PEMFC historical state and operating mode in PEMFC prognosis. *Int. J. Hydrog. Energy* **2020**, *45*, 32355–32366. [CrossRef]
32. An, F.; Zhang, W.; Sun, B.; Jiang, J.; Fan, X. A novel state-of-energy simplified estimation method for lithium-ion battery pack based on prediction and representative cells. *J. Energy Storage* **2023**, *63*, 107083. [CrossRef]
33. Che, Y.; Deng, Z.; Li, P.; Tang, X.; Khosravinia, K.; Lin, X.; Hu, X. State of health prognostics for series battery packs: A universal deep learning method. *Energy* **2022**, *238*, 121857. [CrossRef]
34. Waseem, M.; Lin, Z.; Yang, L. Data-Driven Load Forecasting of Air Conditioners for Demand Response Using Levenberg–Marquardt Algorithm-Based ANN. *Big Data Cogn. Comput.* **2019**, *3*, 36. [CrossRef]
35. Dong, G.; Zhang, X.; Zhang, C.; Chen, Z. A method for state of energy estimation of lithium-ion batteries based on neural network model. *Energy* **2015**, *90*, 879–888. [CrossRef]
36. Waseem, M.; Lin, Z.; Liu, S.; Jinai, Z.; Rizwan, M.; Sajjad, I.A. Optimal BRA based electric demand prediction strategy considering instance-based learning of the forecast factors. *Int. Trans. Electr. Energy Syst.* **2021**, *31*, e12967. [CrossRef]
37. Waqas, A.B.; Ali, Y.; Khan, D.; Faheem, Z.B.; Manan, A.; Shabbir, U. Home energy management strategy for DR accomplishment considering PV uncertainties and battery energy storage system. In Proceedings of the 2021 International Conference on Emerging Power Technologies (ICEPT), Topi, Pakistan, 10–11 April 2021; pp. 1–5.
38. Çelık, D.; Meral, M.E. A New Area Towards to Digitalization of Energy Systems: Enables, Challenges and Solutions. In Proceedings of the 2022 14th International Conference on Electronics, Computers and Artificial Intelligence (ECAI), Ploiesti, Romania, 30 June–1 July 2022; p. 16.
39. Rauf, H.; Khalid, M.; Arshad, N. Machine learning in state of health and remaining useful life estimation: Theoretical and technological development in battery degradation modelling. *Renew. Sustain. Energy Rev.* **2022**, *156*, 111903.
40. Saha, B.; Goebel, K. *Battery Data Set. NASA Ames Prognostics Data Repository*; Moffett Field: Santa Clara, CA, USA, 2007.
41. Gupta, S.; Mishra, P.K. Machine Learning based SoC Estimation for Li-Ion Battery. In Proceedings of the 2023 5th International Conference on Energy, Power and Environment: Towards Flexible Green Energy Technologies (ICEPE), Shillong, India, 15–17 June 2023; pp. 1–6.
42. Li, L.; Jia, S.; Cao, M.; Ji, Y.; Qiu, H.; Zhang, D. Research progress on transition metal sulfide-based materials as cathode materials for zinc-ion batteries. *J. Energy Storage* **2023**, *67*, 107614. [CrossRef]
43. Li, W.; Jiao, Z.; Du, L.; Fan, W.; Zhu, Y. An indirect RUL prognosis for lithium-ion battery under vibration stress using Elman neural network. *Int. J. Hydrog. Energy* **2019**, *44*, 12270–12276. [CrossRef]
44. Li, X.; Yuan, C.; Li, X.; Wang, Z. State of health estimation for Li-Ion battery using incremental capacity analysis and Gaussian process regression. *Energy* **2020**, *190*, 116467. [CrossRef]
45. Liu, D.; Wang, H.; Peng, Y.; Xie, W.; Liao, H. Satellite Lithium-Ion Battery Remaining Cycle Life Prediction with Novel Indirect Health Indicator Extraction. *Energies* **2013**, *6*, 3654–3668. [CrossRef]
46. Wang, H.; Cai, R.; Zhou, B.; Aziz, S.; Qin, B.; Voropai, N.; Gan, L.; Barakhtenko, E. Solar irradiance forecasting based on direct explainable neural network. *Energy Convers. Manag.* **2020**, *226*, 113487. [CrossRef]
47. Roman, R.-C.; Precup, R.-E.; Petriu, E.M.; Muntyan, M. Fictitious Reference Iterative Tuning of Discrete-Time Model-Free Control for Tower Crane Systems. *Stud. Inform. Control.* **2023**, *32*, 5–14. [CrossRef]
48. Sun, L.; Hu, S.J.; Freiheit, T. Feature-based quality classification for ultrasonic welding of carbon fiber reinforced polymer through Bayesian regularized neural network. *J. Manuf. Syst.* **2021**, *58*, 335–347. [CrossRef]

49. Naik, A.; Satapathy, S.C. A comparative study of social group optimization with a few recent optimization algorithms. *Complex Intell. Syst.* **2021**, *7*, 249–295. [CrossRef]
50. Bhatt, B.; Sharma, H.; Arora, K.; Joshi, G.P.; Shrestha, B. Levy Flight-Based Improved Grey Wolf Optimization: A Solution for Various Engineering Problems. *Mathematics* **2023**, *11*, 1745. [CrossRef]
51. Nguyen, T.-H.; Nguyen, L.V.; Jung, J.J.; Agbehadji, I.E.; Frimpong, S.O.; Millham, R.C. Bio-inspired approaches for smart energy management: State of the art and challenges. *Sustainability* **2020**, *12*, 8495. [CrossRef]
52. Waseem, M.; Lin, Z.; Liu, S.; Sajjad, I.A.; Aziz, T. Optimal GWCSO-based home appliances scheduling for demand response considering end-users comfort. *Electr. Power Syst. Res.* **2020**, *187*, 106477. [CrossRef]